https://doi.org/10.5194/egusphere-2022-921
Preprint. Discussion started: 20 September 2022

What drives F_{yw} variations with elevation in Alpine catchments?

Alessio Gentile[1], Davide Canone[1], Natalie Ceperley[4], Davide Gisolo[1], Maurizio Previati[1], Giulia Zuecco[3], Bettina Schaefli[2,4], and Stefano Ferraris[1]

[1]Interuniversity Department of Regional and Urban Studies and Planning (DIST), Politecnico and Università degli Studi di Torino, Torino, Italy
[2]Institute of Earth Surface Dynamic (IDYST), Faculty of Geosciences and Environment (FGSE), University of Lausanne, Lausanne, Switzerland
[3]Department of Land, Environment, Agriculture and Forestry (TESAF), University of Padova, Legnaro, Italy
[4]Institute of Geography (GIUB) and Oeschger Centre for Climate Change Research (OCCR), University of Bern, Bern, Switzerland

Correspondence to: Bettina Schaefli (bettina.schaefli@giub.unibe.ch)

Abstract. The young water fraction (F_{yw}), defined as the fraction of catchment outflow with transit times of less than about 2-3 months, is increasingly used in hydrological studies, replacing the widely used Mean Transit Time (*MTT*), which is subject to aggregation error. The use of this new metric in catchment intercomparison studies is helpful to understand and conceptualize the relevant processes controlling catchment's hydrological function. Past work has shown the remarkable and counterintuitive evidence that steep (and generally high elevation) catchments worldwide reveal small F_{yw} values. However, the topographic slope only partially explains the observed F_{yw} variance, and the mechanisms hidden behind this lowering with slope remain basically unclear.

The main aim of this paper is to investigate what drives F_{yw} variations with elevation in Alpine catchments clarifying why F_{yw} is low at high altitudes. In this regard, we use a dataset composed of 27 study catchments, located both in Switzerland and in Italy, that we categorize as rainfall-dominated, hybrid or snow-dominated according to a proposed formal classification scheme that considers both a common-used monthly streamflow ratio and the snow cover regime. We analyze three not previously investigated variables that could potentially explain the F_{yw} elevation gradients: the fractional snow cover area (F_{SCA}), the fraction of quaternary deposits (F_{qd}), and the fraction of baseflow (F_{bf}). We also consider a fourth variable, namely the Winter Flow Index (*WFI*), for comparing our results about the groundwater contribution to streamflow with those of previous scientific publications.

Our results suggest that unconsolidated sediments could play a role in modulating F_{yw} elevation gradients via their capacity to store groundwater, but further geological information, such as the portion of fractured bedrocks, would be desirable for a complete picture of the role of geology. Based on our analysis concerning the F_{SCA}, we develop a perceptual model that explains how the increasing duration of the snowpack promotes a progressive emptying of the groundwater storage during winter, thereby increasing the streamwater age, while ephemeral snowpack generally favors rapid flow paths that increase F_{yw}. Finally, our work highlights that F_{bf}, considered as a proxy for groundwater flow, is roughly the one's complement of F_{yw}. In harmony with the model, we find high F_{bf} during all low-flow periods, which underlines that streamflow is mainly sustained by groundwater in such flow conditions. For catchments where the winter low-flow period is long compared to the summer high-flow period, this results in low F_{yw}.

In conclusion, our data set suggests that F_{bf} is the best explanatory variable of F_{yw} elevation gradients in Alpine catchments, implying the key-role of major groundwater storages that, with the increasing snowpack duration, are actively involved in streamflow generation processes.

https://doi.org/10.5194/egusphere-2022-921
Preprint. Discussion started: 20 September 2022

1 Introduction

Alpine catchments are assumed to generate a high share of surface runoff due to the presence of exposed bedrock and steep landscapes, consequently the role of groundwater storage in high-elevation catchments has been often neglected (Hayashi, 2020). However, early work in the Swiss Alps showed that high celerity is caused by the release of groundwater to the stream, so that the streamflow is older than the annual snowmelt (Martinec, 1975). This corresponds to results obtained through stable-isotope based hydrograph separation performed in 101 studies worldwide that revealed that more than half of streamflow is composed of groundwater even during no-rain and no-snowmelt periods (Jasechko, 2019). To date, it is well known that the age of water stored in catchments is well beyond the annual timescale and that it plays a key role in streamflow generation processes (McDonnell, 2017; Jasechko, 2019). In this regard, the hydrological community expressed the need for better understanding of transit time distributions in the terrestrial water cycle (Blöschl et al., 2019).

The study of water age is crucial for predicting the timing of nutrient cycles and pollutant transport since water age and solute dynamics can be coupled (Jasechko et al., 2016; Benettin et al., 2017). However, water age quantification is not straight forward. Kirchner (2016a, b) proposed a new metric to quantify water age at the catchment scale: the young water fraction (F_{yw}), defined as the fraction of catchment outflow with transit times of less than roughly 0.2 years (Kirchner, 2016a). It can be conveniently inferred from the dampening effect that a catchment has on the seasonal cycle of stable water isotopes in precipitation, i.e. by estimating the amplitude ratio of the seasonal cycle of stable water isotopes in streamflow to that of precipitation (Kirchner, 2016a). The F_{yw} concept has rapidly supplanted the similar metric, Mean Transit Time (*MTT*), because it has the advantage of being free from the aggregation errors inherent to *MTT*. The F_{yw} is also an informative proxy of a catchment's hydrological function, in terms of water partitioning and release (Stockinger et al., 2019). Therefore, this new metric is useful for catchment intercomparison studies to analyze the main hydro-climatic and landscape characteristics that influence the transit times of water (von Freyberg et al., 2018). Indeed, some studies have already tried to find a relationship between young water fractions and catchment characteristics. von Freyberg et al. (2018) found that young water fractions of 22 Swiss catchments are positively correlated (with statistical significance) with selected hydro-climatic indices and the fraction of saturated area, suggesting that F_{yw} depends on catchment wetness which promotes rapid flow paths.

Interestingly, the analysis by von Freyberg et al. (2018) revealed that the young water fraction is positively correlated with mean catchment elevation, but only when the 5 high-elevation, snow-dominated catchments are omitted from the analysis. Indeed, Ceperley et al. (2020), who compared the F_{yw} from three additional high elevation catchments to the original dataset of von Freyberg et al. (2018), observe a drop of F_{yw} above 1500 m a.s.l., to which we refer hereafter as F_{yw}-reset. In line with these findings, a recent study estimated F_{yw} for 24 catchments in Germany and observed the smallest values in mountainous landscapes (Lutz et al., 2018).

This F_{yw}-reset is partially consistent with the counterintuitive outcomes of Jasechko et al. (2016) whose work reveals that young streamflow is less prevalent in steep (and generally high) landscapes. They explain this by a consistent deep vertical infiltration component for such steep high elevation catchments (Jasechko et al., 2016). However, even if the topographic gradient is correlated with the young water fraction in the 254 watersheds data set of Jasechko et al. (2016), the relationship is relatively scattered, leaving a large portion of variance unexplained and suggesting that other variables can play a key role in reducing F_{yw} according to slope steepness or with elevation (Jasechko et al., 2016).

Comparing different F_{yw} estimation methods in presence of snow in the Swiss and Italian Alps, Ceperley et al. (2020) observed that high Alpine catchments reveal low F_{yw}. Therefore, the snow storage could have a role in decreasing the young water fraction. The elevation of 1500 m a.s.l., above which we have the F_{yw}-reset, has been previously identified

https://doi.org/10.5194/egusphere-2022-921
Preprint. Discussion started: 20 September 2022

as corresponding to the transition between intermittent and seasonal snow cover (Santos et al., 2018). However, it is unclear if the snow cover dynamics can lead to a more efficient groundwater recharge, consequently reducing or increasing the young streamflow reaching the stream (Ceperley et al., 2020).

Tracer or water balance methods are powerful tools to quantify groundwater contribution to rivers and multiple worldwide studies have estimated the considerable groundwater input to streamflow in high mountain catchments using such methods (Somers and McKenzie, 2020). Several catchments located in the Rocky Mountains and Andes mountain ranges show that remarkable fractions of groundwater annually sustain the streamflow (Saberi et al., 2019; Somers et al., 2019; Carroll et al., 2018; Harrington et al., 2018; Cowie et al., 2017; Baraer et al., 2015; Gordon et al., 2015; Frisbee et al., 2011; Liu et al., 2004; Clow et al., 2003; Baraer et al., 2009). This result is also found in the Himalayas and Alps mountain ranges (Chen et al., 2018; Engel et al., 2016; Käser and Hunkeler, 2016; Williams et al., 2016; Wilson et al., 2016; Andermann et al., 2012). There is however still a lack of understanding regarding the mechanisms that lead to a dynamic storage contribution to streamflow (Kirchner, 2003) and, consequently, how this contribution impacts the young water fraction.

Moreover, recent streamflow data-based and model-based studies in the Swiss Alps point towards important mobile groundwater storage in high elevation catchments, which could be related to quaternary deposits: e.g., moraines, alluvium, and talus (Staudinger et al., 2017; Cochand et al., 2019; Arnoux et al., 2021). Therefore, it is necessary to understand the capability of unconsolidated sediments of storing high-mountain groundwater and how this geology influences the amount of young water reaching the stream.

Accordingly, we study here a new set of hydrological variables to gain new insights into the F_{yw} along elevation gradients: the fractional snow cover area (F_{SCA}), the fraction of quaternary deposits (F_{qd}) and the fraction of baseflow (F_{bf}), defined in detail in Sections 3.4 and 3.5. We also consider a fourth index, namely the Winter Flow Index (*WFI*), for testing consistency of our results with those of a past study (Arnoux et al., 2021) that used this index to quantify the groundwater contribution to streamflow.

In the following, we first classify the study catchments, described in Section 2, into three hydro-climatic regimes proposing a new criterion of classification (Section 3.3). Then, we study the correlation of the selected hydrological variables with the young water fraction (Sections 4.3.1, 4.3.2, 4.3.3) and we finally bring these results back to the ongoing scientific discussion of F_{yw} (Section 5).

2 Study sites

In this work we analyze 27 study catchments located both in Switzerland and Italy (Table S1, Fig. 1) and integrate observations from multiple published existing datasets (25 catchments) with new additional observations (2 catchments).

2.1 Existing dataset

Initial, we integrate the 22 Swiss catchments studied by von Freyberg et al. (2018) with the three Alpine catchments (Vallon de Nant, Noce Bianco at Pian Venezia and Bridge Creek Catchment) investigated by Ceperley et al. (2020) into a single dataset. Time series of both δ^2H and $\delta^{18}O$ in streamflow and precipitation for the 22 Swiss catchments are reported and described by Staudinger et al. (2020). Furthermore, 21 out of the 22 Swiss catchments were also considered in a previous study (which did not consider the Alp catchment) that analyzed the variation of the catchment water storage with elevation (Staudinger et al., 2017). In turn, daily isotope measurements for the Alp (ALP) catchment and its two tributaries, Erlenbach (ERL) and Vogelbach (VOG) catchments, were thoroughly described by von Freyberg et al. (2022).

https://doi.org/10.5194/egusphere-2022-921
Preprint. Discussion started: 20 September 2022

Two high-elevation catchments among the 22, namely Dischmabach (DIS) and Ova da Cluozza (OVA), were also investigated in previous studies for climate change impact predictions, low-flow analysis and for understanding the role of quaternary deposits and groundwater in their hydrological functioning (Addor et al., 2014; Staudinger and Seibert, 2014; Staudinger et al., 2015; Jenicek et al., 2018; Arnoux et al., 2021). Among the catchments analyzed by Ceperley et al. (2020), the reader is referred to Michelon et al. (2022) for further information about the tracer-based dynamics of the Vallon de Nant (VdN) catchment and to Carturan (2016), Carturan et al. (2013, 2014, 2016, 2019), Zuecco et al. (2019) for glaciological, hydrological and meteorological information about the Noce Bianco at Pian Venezia (NBPV) catchment. Additional details for the dolomitic Bridge Creek Catchment (BCC) are available in the work of Zuecco et al. (2018, 2019), Guastini et al. (2019) and Penna et al. (2016, 2017).

2.2 Additional dataset

We consider two additional high-elevation catchments located near the Nivolet Pass (Valsavaranche, Aosta Valley, Italy) in a high-elevation grassland within the Gran Paradiso National Park territory (Gisolo et al., 2022). The mainstream is the Dora del Nivolet. Hereafter we refer to this catchment simply as "Dora" (DOR). DOR has a catchment area of 17 km^2 and its elevation ranges from 2390 to 3430 m a.s.l. Average annual precipitation in the period 2017-2021 was 2164 mm. It experiences a snow-dominated hydro-climatic regime with the snowpack generally persisting from mid-November to mid-May when the snowmelt starts. Since the snowpack melts during the growing season, it uncovers a typical alpine meadow home to plant species including Gentiana Lutea L., Juniperus Communis L., Vaccinium Myrtillus L., Salix Alpina Scop. and Trifolium Alpinum L. The lithology of DOR is dominated by gneiss. Bedrock emerges at high elevations, while at medium elevations the talus dominates. At lower elevations we find the alpine meadow, characterized by peat substrate, through which the mainstream flows. We monitor precipitation every month with a rain gauge located at roughly 2560 m a.s.l. We measure streamflow continuously (10 min timestep) at the DOR outlet point and in a lateral subcatchment, on the left bank of the mainstream, using piezo-resistive multi-sensors. We call this lateral subcatchment "Source" (SOU), since it is characterized by water emerging from underground. The SOU subcatchment extends for roughly 0.16 km^2 and its elevation ranges from 2390 to 2790 m a.s.l. Water samples for isotopic analysis are collected of both bulk precipitation and streamwater at a monthly time resolution. Specifically, precipitation samples were collected using a double rain and snowfall isotope sampler installed on a pole 3.7 m high, near the rain gauge, while streamwater was sampled manually (Fig. S1). All precipitation and streamwater samples were analyzed with laser spectroscopy at the Forest Hydrology laboratory of University of Padova.

2.3 Complete dataset

The von Freyberg et al. (2018) dataset includes catchments with areas between 0.7 and 351 km^2 and mean elevations between 472 and 2369 m a.s.l. Average annual precipitation in these catchments ranges from 887 to 2615 mm. With the data added here, the entire dataset now covers areas between 0.14 and 351 km^2 and has mean elevations between 472 and 3049 m a.s.l. Specifically, the additional 5 catchments added to the initial dataset of von Freyberg et al. (2018) allow analysis to explore the high-elevation (i.e., > 1500 m a.s.l.) regions that were previously poorly represented. Furthermore, the complete dataset now includes case studies from five different Alpine regions, including the Northern part of the Swiss Alps, the Southern Swiss Alps (Alpi Ticinesi), the Western Italian Alpes (Alpi Graie), the Rätische Alpen and the Dolomites. This represents a good range of geologies as well as of climatic conditions, as visible from Table 1.

https://doi.org/10.5194/egusphere-2022-921
Preprint. Discussion started: 20 September 2022

Like von Freyberg et al. (2018), we classify the catchments in the three hydro-climatic regimes (snow-dominated, hybrid and rainfall-dominated) proposed by Staudinger et al. (2017), but we introduce a new formal criterion of classification (see Section 3.3).

The geographical framework of the selected catchments is illustrated in Fig. 1 and their geomorphological and climatic characteristics are reported in Table 1.

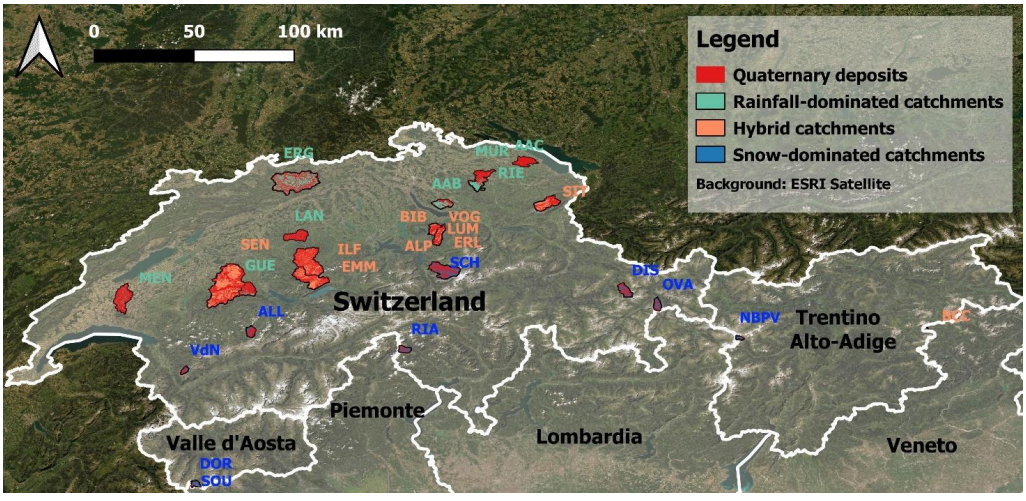

Figure 1. Location of the 27 study catchments with indication of hydro-climatic regime and quaternary deposits coverage discussed in Section 4.2 and Section 4.3.2.

Table 1. Catchments geomorphological and climatic characteristics. Catchments area and average slope are directly calculated in Google Earth Engine. For the slope calculation we use the Shuttle Radar Topography Mission (SRTM) DEM. We obtained elevation and annual precipitation information of the existing dataset directly from published papers (Staudinger et al., 2017; von Freyberg et al., 2018; Ceperley et al., 2020).

ID	Area (km^2)	Average Elevation (m a.s.l.)	min Elevation (m a.s.l.)	max Elevation (m a.s.l.)	Average Slope (°)	Dominant geology	Annual Prec. (mm)
AAB	46.07	635	519	1092	5.73	Sediment. Rock (upper freshwater molasse)	1081
AAC	47.25	472	408	560	4.02	Unconsolidated sediments (moraine)	1095
ALL	28.71	1852	1293	2742	25.48	Sediment. Rock and unconsolidated sediments (flysch, sandstones, profound weathering soils, avalanche debris, hanging rubble and cones of dry rubble)	1651
ALP	46.59	1154	845	1894	16.50	Sediment. Rock and unconsolidated sediments (flysch, conglomerates, sandstones, marls, carbonate-rich molasse, alluvions)	2112
BCC	0.14	2121	1932	2515	22.88	Dolomite	1203
BIB	31.83	999	827	1495	12.43	Sediment. Rock and unconsolidated sediments (conglomerates, sandstones, marls, carbonate-rich molasse, Grindelegg-	1639

https://doi.org/10.5194/egusphere-2022-921
Preprint. Discussion started: 20 September 2022

						series, granitic molasse, Torfmoor, alluvions, moraine)	
DIS	42.75	2369	1663	3139	26.28	Metamorphic rock (metagranitoids, amphibolites, mica shist, gneiss, moraine)	1391
DOR	16.99	2711	2390	3430	19.37	Metamorphic rock (gneiss, amphibolites, alluvions)	2164
EMM	124.03	1285	743	2216	19.71	Sediment. Rock (mediterranean molasse, subalpine molasse, ground lime formation, calcareous quartz sandstone, moraine, hanging rubble, cone of dry rubble)	1559
ERG	260.47	584	305	1165	13.86	Sediment. Rock (conglomerate, sandstone, subordinately siltstone, marl, crust limestone, oolitic, peloidal and micritic limestone, Staffelegg-formation, Opalinus-Ton,scree)	1012
ERL	0.74	1359	1117	1650	13.53	Sediment. Rock (flysch, eboulis)	2168
GUE	55.23	1037	556	2152	16.84	Sediment. Rock and unconsolidated sediments (flysch, eboulis, dry cones, Sequanian, moraine)	1241
ILF	186.94	1037	681	2087	19.36	Sediment. Rock (colorful polymictic conglomerate subordinate to sandstone and marl or silty marl, mediterranean molasse, flysch subalpine, alluvions)	1450
LAN	59.76	760	598	1100	10.08	Sediment. Rock (Napf formation and St. Gallen formation under thin quaternary cover, Dürrenroth gravel, alluvions)	1195
LUM	1.20	1336	1092	1508	12.49	Sediment. Rock (flysch)	2615
MEN	105.02	679	447	926	6.19	Sediment. Rock and unconsolidated sediments (variegated sandstone and marl under thin morainic cover, sandstone and marl, moraine)	1060
MUR	79.92	648	467	1036	10.52	Sediment. Rock and unconsolidated sediments (upper freshwater molasse, moraine, postglacial gravel)	1281
NBPV	8.39	3049	2298	3769	23.27	Metamorphic and sediment. rock (phyllites, paragneiss, parascists)	1413
OVA	26.87	2364	1519	3160	32.73	Dolomite	887
RIA	23.85	1986	881	2908	32.93	Metamorphic rock (Biotite, granodiorite, gneiss, mica shist, hanging rubble and cones of dry rubble)	2104
RIE	3.18	794	671	938	13.23	Sediment. Rock and unconsolidated sediments (upper freshwater molasse, moraine)	1555

https://doi.org/10.5194/egusphere-2022-921
Preprint. Discussion started: 20 September 2022

SCH	107.61	1719	487	3260	28.78	Sediment. Rock and unconsolidated sediments (flysch, settling mass, rockslide, moraine)	1687
SEN	350.24	1068	554	2184	15.35	Sediment. Rock (flysch, sandstone, marls, scists, moraine)	1270
SIT	74.23	1301	768	2500	22.15	Sediment. Rock (lower freshwater molasse, Helvetian calcareous limestone, lower Schrattenkalk, moraine)	1870
SOU	0.16	2636	2390	2790	25.74	Metamorphic rock (gneiss)	2164
VdN	13.55	1966	1189	3051	34.00	Sediment. Rock (flysch, sandstone, marls)	1591
VOG	1.57	1335	1038	1540	18.42	Sediment. Rock (flysch)	2161

3 Material and Methods

3.1 Discharge data and catchments boundaries

Daily discharge data for the Erlenbach (ERL), Lümpenenbach (LÜM) and Vogelbach (VOG) catchments are provided by the *Swiss Federal Institute for Forest, Snow and Landscape research* (*WSL*), Birmensdorf, Switzerland. Moreover, streamflow data for the Aabach (AAB) and Guerbe (GUE) catchments are provided by the *Office for Waste, Water, Energy and Air* (*WWEA*) of the Canton of Zurich and by the *Office for Water and Waste* of the Canton of Bern, respectively. Vallon de Nant (VdN) 1-min discharge measurements are obtained via an optical height gauge above the middle point of a trapezoid shape weir (Antoniazza et al., 2022; Michelon et al., 2022), and they are subsequently aggregated to daily streamflow values. Bridge Creek Catchment (BCC) and Noce Bianco at Pian Venezia (NBPV) catchment daily streamflow data are provided by Dr. Giulia Zuecco, (University of Padova, Italy). Daily discharge data for the DOR and SOU catchments are obtained aggregating 10-min measurements deriving from piezo-resistive multi-sensors (as described in Section 2). Daily discharge data of the remaining 17 Swiss catchments studied by von Freyberg et al. (2018) are provided by the *Swiss Federal Office for the Environment* (*FOEN*).

We obtain the .shp of the AAB, GUE, ERL, LÜM and VOG catchments boundaries from the Zenodo data repository reported in Staudinger et al. (2020); the .shp of NBPV, BCC and VdN catchments, are provided by Dr. Giulia Zuecco and Dr. Anthony Michelon (University of Lausanne, Switzerland) as personal communication. We delineate the DOR and SOU catchments boundaries in a GIS environment using the 10-m resolution Digital Elevation Model (DEM) available from the *Aosta Valley Regional Geoportal*. Finally, we obtain the catchment boundaries of the remaining 17 Swiss catchments investigated by von Freyberg et al. (2018) directly from the *Swiss Federal Office for the Environment* (*FOEN*).

3.2 Young water fraction estimation from seasonal cycles of stable water isotopes in precipitation and streamwater

Kirchner (2016a) has demonstrated that the F_{yw} can be easily approximated by the amplitude ratios of seasonal sine curves fitted to streamwater and precipitation isotope values. Operatively, seasonal isotope (e.g., $\delta^{18}O$) cycles in streamwater and precipitation can be modelled by:

$$\delta^{18}O_S(t) = A_S \sin(2\pi f t - \varphi_S) + k_S\,, \quad (1)$$

https://doi.org/10.5194/egusphere-2022-921
Preprint. Discussion started: 20 September 2022

$$\delta^{18}O_P(t) = A_P \sin(2\pi f t - \varphi_P) + k_P \,, \quad (2)$$

where, $\delta^{18}O$ (‰) is the isotopic composition of water sampled at the time t (expressed in decimal years), A (‰) is the amplitude of the seasonal isotope cycle, φ (in radians) is the phase, f (yr^{-1}) is the frequency and k (‰) is the vertical offset of the seasonal isotope cycle. The subscript "S" refers to streamwater, while the subscript "P" refers to precipitation. As in the work of Kirchner (2016a), we fit the sine curves of Eq. (1) and Eq. (2) on the isotope measurements using the *Iteratively Re-weighted Least Squares* (*IRLS*) method (for reducing the influence of outliers) and then estimate the A, φ and k parameters.

Thus, following Kirchner (2016a), it is possible to calculate the young water fraction via the "amplitude ratio approach":

$$F_{yw} = \frac{A_S}{A_P} \,. \quad (3)$$

We fit a sine wave to the isotopes measured in precipitation according to volume of precipitation to reduce the influence of low-precipitation periods and to account for temporally aggregated rainfall samples (von Freyberg et al., 2018); the sine-fit of streamwater isotope measurements can be discharge-weighted or not, using the discharge measured at the moment of sampling as weights (von Freyberg et al., 2018). Consequently, we obtain an unweighted A_S or a flow-weighted A_S with which Eq. (3) can be evaluated. The uncertainty of these estimated F_{yw} (flow-weighted or unweighted) are calculated using the Gaussian error propagation (von Freyberg et al., 2018). Flow-weighting was used in both the work of von Freyberg et al. (2018) and Ceperley et al. (2020). Gallart et al. (2020) highlighted the advantages of the flow-weighted analysis (generally yielding flow-weighted A_S greater than unweighted A_S) to compensate for subsampled high-flow periods. Thereby, for the existing dataset, we consider the values of flow-weighted F_{yw} reported in Table 3 of von Freyberg et al. (2018) and in Table 6 of Ceperley et al. (2020) with associated errors.

Accordingly, for the additional dataset composed by the DOR and SOU catchments, we apply the procedure above for calculating the flow-weighted F_{yw} using $\delta^{18}O$ measurements collected in the period November 2017 - January 2022.

3.3 A new hydro-climatic regime classification: the classifiers

Our analysis focuses on Alpine catchments whose streamflow regimes are dominated by natural precipitation-runoff transformation processes. The corresponding streamflow regimes are classically divided into those that are rainfall-driven (often called pluvial) and those that are snow-dominated, with or without glacier influence and possibly including hybrid regimes (Weingartner and Aschwanden, 1992; Moore et al., 2012; Staudinger et al., 2017).

While the streamflow regime terminology is omnipresent in hydrology literature, there is often no formal classification method provided (Déry et al., 2009). Switzerland has a formal streamflow regime classification into 16 regimes, largely based on Pardé coefficients (Pardè, 1933), i.e. monthly streamflow ratios (Weingartner and Aschwanden, 1992), used by a few additional authors (Curran and Biles, 2021). Some authors consider mean catchment elevation or human influence (Piccolroaz et al., 2016). These classifications are typically based on streamflow data and some topographical data (e.g., elevation and glacier cover).

We design a new criterion, explained below, for classifying streamflow regimes as rainfall-dominated, hybrid and snow-dominated, which should be as parsimonious as possible (i.e., using few explicative variables) and account explicitly for the snow cover regime in the catchments. As a proxy for the snow cover regime, we use the average fractional Snow Cover Area (F_{SCA}): we discuss its computation in Section 3.4. Staudinger et al. (2017) classify the catchments in the above-mentioned clusters grouping some of the regimes defined by Weingartner and Aschwanden (1992) that are built on the streamflow regime in Switzerland. The tricky-points of this "three regimes classification" are the transitions, both from rainfall-dominated to hybrid catchments and, similarly, from hybrid to snow-dominated ones. Focusing on these

https://doi.org/10.5194/egusphere-2022-921
Preprint. Discussion started: 20 September 2022

transitions, in both cases, we reason that the role of snowpack is crucial. From our knowledge of the regime classification systems already existing in literature, there are no studies that explicitly consider the role of snow. Expansion in satellite data ubiquity, frequency, and accessibility has rendered the assessment of snow cover only recently feasible.

For the classification, we further use a common monthly streamflow ratio, namely the Q_{June}/Q_{DJF} ratio (i.e., ratio of the average flow of June and the sum of average flow of December, January, and February), as a classifier. Flow is relative to catchment area; it is expressed in mm per time step. Using the regime classification of Staudinger et al. (2017) as a base, we compare the monthly streamflow of their catchments belonging to different regimes and we focus thereby on Q_{DJF} (as proxy for winter flow) and Q_{June} (as a proxy for summer flow). It is in fact during these two periods that Q_{June} and Q_{DJF} differ the most between different regime types, as shown in Fig. 2. Accordingly, our new classification scheme (Section 4.2) is based on two variables: the F_{SCA} and Q_{June}/Q_{DJF} ratio.

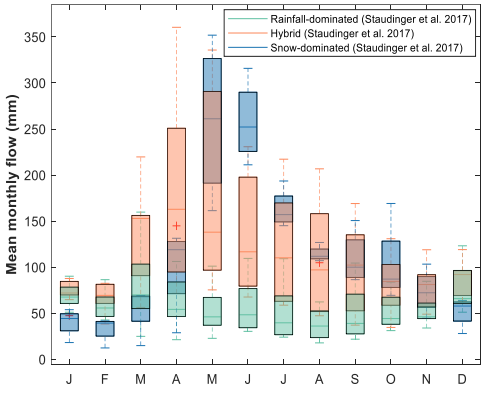

Figure 2. Boxplots of mean monthly flow for catchments studied by Staudinger et al. (2017) and grouped according to their flow-regime classification (rainfall-dominated, hybrid, snow-dominated)

3.4 Average fractional Snow Cover Area (F_{SCA}) computation

The F_{SCA} for each catchment is calculated over the period October 1st 2017- September 30th 2021 (hereafter defined as *PoI*, i.e., Period of Interest) starting from Sentinel-2 L2A satellite images. Temporally, this relatively recent satellite has increased the visitation frequency to more than weekly and increased the spatial resolution to 20 m for snow cover (Gascoin et al., 2019). High temporal resolution makes Sentinel-2 images preferable to Landsat images, which are available only once every 16 days and whose total number is often further reduced because of cloudiness (Hofmeister et al., 2022). For each image available in the *PoI*, we calculate the Normalized Difference Snow Index (*NDSI*) as suggested in the work of Dozier (1989):

$$NDSI := \frac{r_{green} - r_{SWIR}}{r_{green} + r_{SWIR}}, \quad (4)$$

where r_{green} is the reflectance in the green band (Sentinel-2 band 3) and r_{SWIR} is the shortwave infrared reflectance band (Sentinel-2 band 11). We classify as snowy pixels those with a *NDSI* value > 0.4 (Dozier, 1989). Based on the pixel-wise snow classification, we compute f_{SCA} as in the works of Di Marco et al. (2020) and Hofmeister et al. (2022):

$$f_{SCA} = \frac{N_{snow}}{N_{tot} - N_{clouds}}, \quad (5)$$

where N_{snow} is the number of snow cover pixel according to the applied *NDSI* threshold method, N_{tot} is the total number of pixels within the catchment area and N_{clouds} is the number of pixels classified as cloud and water bodies (Hofmeister et

https://doi.org/10.5194/egusphere-2022-921
Preprint. Discussion started: 20 September 2022

al., 2022). We identify the cloudy pixels directly using the Sentinel-2 band "Scene Classification Map". We operatively calculate N_{snow}, N_{tot} and N_{clouds} using a Google Earth Engine script.

Using this procedure for calculating f_{SCA}, we sometimes obtain $f_{SCA} > 1$, typically for winter satellite images. The *NDSI* threshold method is generally able to distinguish between snow and no-snow pixels (Aalstad et al., 2020). Accordingly, clouds and snow have similar reflectance in the green band, but clouds highly reflect in the shortwave infrared band, while snow reflectance is low in this band. Thus, the N_{snow} estimation is generally accurate. On the other hand, it is necessary to reduce the number of false positive pixels deriving from clouds detection (i.e., snow classified as clouds).

During winter it is likely that N_{snow} approaches very close to N_{tot}. Accordingly, it is easy to have N_{tot}-$N_{clouds} < N_{snow}$ if N_{clouds} incorporate pixels that are in fact snow covered. In these cases, we assume that $N_{clouds} = N_{tot}$-N_{snow} (i.e., f_{SCA} =1). Moreover, by looking at sample Sentinel-2 images during the summer periods for all the catchments, we impose $f_{SCA} = 0$ during July and August, since when f_{SCA} other than 0 has usually falsely identified clouds as snow; imposing $f_{SCA} = 0$ clearly leads to fewer errors (missed occasional summer snowfall events of very shallow depth) than falsely accounting for (far more) frequent clouds. The Noce Bianco Pian Venezia (NBPV) catchment is an exception since it generally has snow over the glacier also during summer. Finally, we remove small inaccuracies by applying a moving average on a window of three images over the f_{SCA} timeseries.

After this filtering step, we compute the average f_{SCA} (i.e., F_{SCA}) for each catchment by averaging all f_{SCA} values available for all snow images in the *PoI*, without interpolation between the time steps.

3.5 Accounting for groundwater: fraction of quaternary deposits (F_{qd}), Winter Flow Index (*WFI*) and baseflow fraction (F_{bf})

Some authors have revealed the key possibility of unconsolidated sediments (e.g., talus, moraine, alluvium) storing groundwater in Alpine catchments (Christensen et al., 2020; Hayashi, 2020; Arnoux et al., 2021). The stored water in these deposits can in fact sustain streamflow during the low-flow period (Hayashi, 2020; Arnoux et al., 2021), i.e. during long periods without direct water input, especially during winter, which can last 6 months or more in high elevation catchments. Such sustained flow during long periods points towards important amounts of stored water that is well connected to the streamflow network and thereby remains accessible throughout the low flow period and also during glacier and snowpack recession due to climate change (Somers et al., 2019). It is thus natural to think that groundwater might also play a key role in driving F_{yw} in Alpine catchments.

We describe in this section how to calculate three quantities that are all, directly or indirectly, linked to groundwater: fraction of quaternary deposits (F_{qd}), the Winter Flow Index (*WFI*) and baseflow fraction (F_{bf}). First, we estimate the proportion of quaternary deposits similarly to Arnoux et al. (2021). Operatively, for the 23 Swiss catchments of our dataset, we calculate the portion of the catchment area occupied by quaternary deposits using the Geological Atlas of Switzerland (GeoCover dataset, 1:25000 scale) freely available from the *Federal Office of Topography swisstopo*. We use the geological sheets that intersect the catchments boundaries for evaluating the portion of unconsolidated sediments area (A_{qd}) covering the catchments area (A). Thus, we calculate the fraction of quaternary deposits (F_{qd}) as:

$$F_{qd} = \frac{A_{qd}}{A}. \quad (6)$$

We repeated the same procedure for the DOR and SOU catchments by using the regional geological map for obtaining this fraction. For the DOR and SOU catchments the vectorized Valsavaranche geological map (1:100000 scale) is provided by the *Cartography Office* of *SCT Geoportal*. For the NBPV and BCC catchments the .shp of unconsolidated

https://doi.org/10.5194/egusphere-2022-921
Preprint. Discussion started: 20 September 2022

sediments is provided by Dr. Giulia Zuecco. The spatial cover of quaternary deposits for the 27 study catchments is reported in Fig. 1.

To complement geological information, we also calculate the Winter Flow Index (*WFI*), a low-flow indicator that is generally used to evaluate the potential of catchments to store groundwater (Paznekas and Hayashi, 2016; Cochand et al., 2019; Hayashi, 2020; Arnoux et al., 2021):

$$WFI := \frac{Q_{NM7}}{Q_{mean}}, \quad (7)$$

where Q_{NM7} is the minimum discharge over seven consecutive days during the winter period (from November to June) and Q_{mean} is the mean annual discharge (Arnoux et al., 2021).

Finally, we estimate the baseflow contribution to streamflow that is generally assimilated to the flow from groundwater and, accordingly, is associated to groundwater processes (Hall, 1968; Duncan, 2019). Additionally, Duncan (2019) provides a specific technique that allows estimation of separate components with physical relevance in the case that baseflow separation techniques were not applied to describe physical processes. We apply the baseflow separation technique described by Duncan (2019) to the discharge time series of the 27 study catchments. Specifically, we apply it to the available discharge measurements within the temporal windows of streamwater isotope sampling. For the 22 Swiss catchments from von Freyberg et al. (2018), we consider the sampling period reported in Table 1 of their published paper. For VdN, NBPV and BCC catchments we consider the time windows November 2015 - December 2018, May 2013 - September 2015, March 2010 - October 2017, respectively. Finally, for the DOR and SOU catchments, we consider discharge measurements in the period November 2017 - January 2022. To express the groundwater contribution to streamflow in a form that is directly comparable with the young water fraction, we define the baseflow fraction (F_{bf}) as:

$$F_{bf} = \frac{1}{n}\sum_{i=1}^{n}\frac{Q_{bf}(t_i)}{Q(t_i)}, \quad (8)$$

where Q_{bf} is the amount of daily baseflow (mm d^{-1}) we obtain using the baseflow separation technique described in the work of Duncan (2019), Q is the daily discharge (mm d^{-1}), t_i is the time step for which we have discharge measurements (where the subscript "i" refers to a specific day) and n is the total number of days within the considered time window.

4 Results

4.1 Young water fraction estimation for DOR and SOU catchments

We apply the methodology described in Section 3.2 to estimate the young water fraction in DOR and SOU catchments. The unweighted F_{yw} values are equal to 0.1 ± 0.02 for both DOR and SOU catchments. In contrast, the flow-weighted F_{yw} are 0.16 ± 0.03 and 0.01 ± 0.02 for DOR and SOU catchments, respectively. Thus, we find a 60% increase of the flow-weighted F_{yw} for the main catchment, while flow-weighted F_{yw} remains unchanged for the very small lateral subcatchment. The F_{yw} results for these two high-elevation catchments agree with F_{yw} estimated by Jasechko et al. (2016), Lutz et al. (2018), Ceperley et al. (2020), who found less young streamflow in mountains than in other landscapes.

4.2 The new hydro-climatic regime classification

Two selected variables, Q_{June}/Q_{DJF} and F_{SCA}, classify catchments into three classes using our streamlined methodology: rainfall-dominated, hybrid and snow-dominated; these have the same names as the ones proposed by Staudinger et al. (2017) but the classification is not based on the same criteria.

In order to achieve a classification as consistent as possible with that of Staudinger et al. (2017), but based on these two variables, we propose the thresholds presented in Table 2:

https://doi.org/10.5194/egusphere-2022-921
Preprint. Discussion started: 20 September 2022

Table 2. New formal classification scheme for defining the catchments hydro-climatic regime using two variables: the F_{SCA} and Q_{June}/Q_{DJF} ratio.

Condition 1	logical	Condition 2	Hydro-climatic regime
$Q_{June}/Q_{DJF} \leq 1$	&	$F_{SCA} < 0.3$	Rainfall-dominated
$Q_{June}/Q_{DJF} \leq 1$	&	$0.3 \leq F_{SCA} \leq 0.5$	Hybrid
$Q_{June}/Q_{DJF} > 1$	&	$F_{SCA} \geq 0.5$	Snow-dominated

The catchment's hydro-climatic regimes defined with these thresholds for the two variables or classifiers are generally consistent with those of Staudinger et al. (2017) (Table S1). The only exceptions are the BIB and GUE catchments whose regimes switch from rainfall-dominated to hybrid (BIB) and vice-versa (GUE). The hydro-climatic regime switch arises for these two catchments because their Q_{June}/Q_{DJF} ratio are < 1, while their F_{SCA} (0.32 for BIB and 0.29 for GUE) are very close to our selected threshold of 0.3. Following our classification scheme, the 27 study catchments are equally distributed over the three classes: 8 rainfall-dominated catchments, 10 hybrid catchments and 9 snow-dominated catchments. The regime of each catchment is reported in Table S1.

The two selected classifiers are positively correlated ($\rho_{Spearman}$ = 0.89 p-value < 0.01). Moreover, fitting an exponential model ($a\ e^{bF_{SCA}}$) on the Q_{June}/Q_{DJF} vs F_{SCA} points, we obtain a = 0.03 (confidence bounds: 0.02 ÷ 0.04) and b= 8.32 (confidence bounds: 7.95 ÷ 8.70) with a very high R^2 = 0.99 (Fig. 3, the 95% confidence bounds of the coefficients are obtained through a robust fit using the bisquare weighting function in Matlab R2019b). This result suggests that the easy-to-calculate Q_{June}/Q_{DJF} ratio is a good predictor of the snow regime, here represented by F_{SCA}. Thus, if F_{SCA} data are missing, it is possible to use the exponential relationship (Fig. 3) for a first order estimate of the second classifier. Some catchments, specifically SCH, ILF and EMM fall away from the curve. They are hybrid or snow-dominated catchments with large areas (> 100 km^2) and wide elevation ranges (> 1400 m). In such cases the summer flow is more influenced by summer rainfall at lower elevations and snowmelt preferentially occurs during spring, reducing the Q_{June}/Q_{DJF} ratio. For catchments with these characteristics, the use of the exponential relationship underestimates the F_{SCA}.

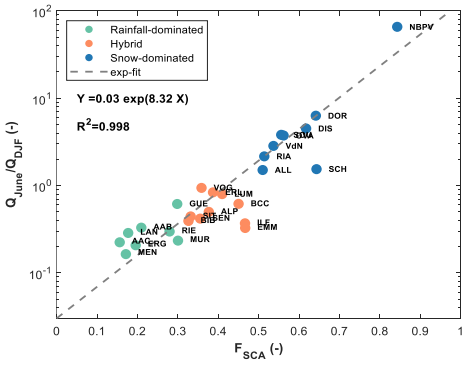

Figure 3. Scatterplot of the 2 selected classifiers: Q_{June}/Q_{DJF} and F_{SCA}. It shows the strong correlation between the two classifiers.

4.3 New explanatory variables for the F_{yw} elevation gradients

Initial evidence of low F_{yw} in high-elevation catchments is given in the work of Jasechko et al. (2016). Based on the analysis of 254 worldwide watersheds, their work reveals a reduction of F_{yw} in steeper terrains. A first physical explanation of this result could be related to deep vertical infiltration caused by fractures generated by the high stress that rocks have to endure in complex terrain morphologies such as those of high-elevation environments (Gleeson et al., 2014;

https://doi.org/10.5194/egusphere-2022-921
Preprint. Discussion started: 20 September 2022

Jasechko et al., 2016). Moreover, the higher the topographic roughness is, the longer are the flow paths, with a consequent rise of transit time (Gleeson and Manning, 2008; Frisbee et al., 2011; Jasechko et al., 2016)

Our dataset is characterized by a general increase of slope with elevation (Fig. 4a). Despite this, we do not find significant correlation between F_{yw} and mean slope ($\rho_{Spearman}$ = -0.25, p-value = 0.22) (Fig. 4b). The correlation becomes significant only when the rainfall-dominated catchments are removed from the analysis ($\rho_{Spearman}$ = -0.7 p-value < 0.01). This result suggests that there is an increasing rate of infiltration when the hydro-climatic regime transitions from hybrid to snow-dominated. We probed deeper into the role of snow and groundwater in lowering the F_{yw} to understand the hydrological function of these focus catchments.

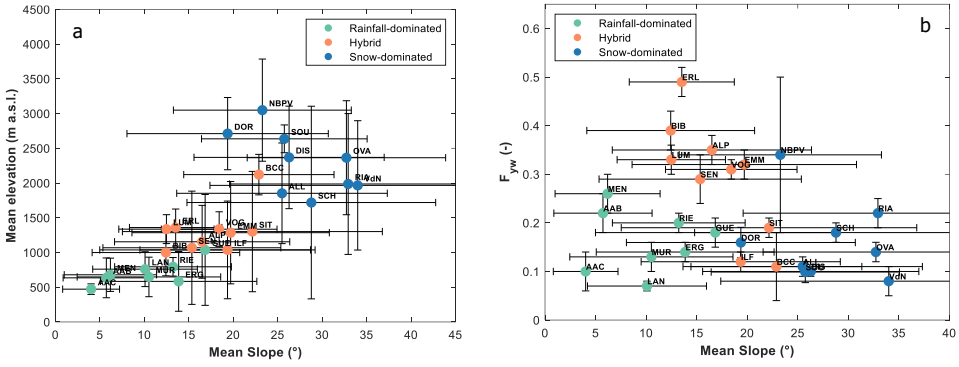

Figure 4. a) Catchments plotted according to mean elevation and mean slope. The vertical bars correspond to the elevation range (i.e., max elevation minus minimum elevation). The horizontal bars correspond to +/- standard deviation b) Young water fractions against mean slope. The horizontal and vertical bars correspond to the uncertainty range (+/- standard deviation) given in the original sources or calculated here for DOR and SOU catchments.

4.3.1 Fractional Snow Cover Area (f_{SCA}) and F_{yw}

The f_{SCA} timeseries for six representative study catchments (two for each hydro-climatic regime) are reported in Fig. 5, whereas the timeseries for all the study sites are available in the Supplementary Material (Fig. S2).

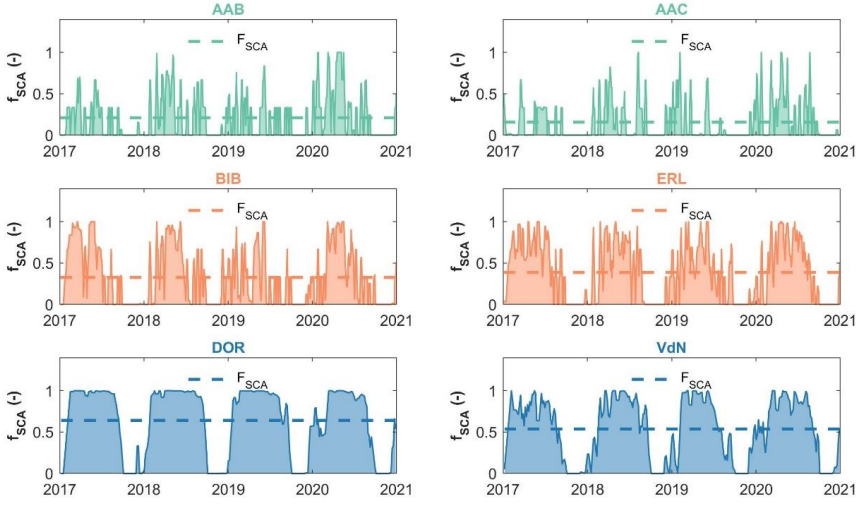

Figure 5. Timeseries of f_{SCA} for 6 representative study catchments (two for each hydro-climatic regime), illustrating the gradual increase of the F_{SCA} passing from rainfall-dominated to snow-dominated catchments.

https://doi.org/10.5194/egusphere-2022-921
Preprint. Discussion started: 20 September 2022

As stated above, we calculate the F_{SCA} as a proxy of the snow-regime. High F_{SCA} values (> 0.5) correspond to catchments with a seasonal snow cover (i.e., catchments where the snowmelt events are concentrated during late spring and summer). Gradually smaller F_{SCA} values refer to increasingly more ephemeral snowpacks, with intermittent snowmelt events during the winter season (Petersky and Harpold, 2018), as reflected by the spiky f_{SCA} timeseries of hybrid and rainfall-dominated catchments (Fig. 5).

Our results highlight a different median F_{yw} for each hydro-climatic regime (Fig. 6), with similar low values for rainfall-dominated catchments (median F_{yw} of 0.16) and snow-dominated catchments (median F_{yw} of 0.14) but much higher values for hybrid catchments (median F_{yw} of 0.32), which in addition shows higher dispersion (Fig. 6). We observe a general increase of F_{yw} as long as the F_{SCA} remains below roughly one third or more exactly 0.38 (median f_{SCA} for hybrid catchments) and a subsequent lowering of F_{yw} when F_{SCA} is higher than this threshold. In fact, considering only catchments with a $F_{SCA} < \approx 0.38$, we obtain a statistically significant positive correlation between F_{yw} and F_{SCA} ($\rho_{Spearman}$ = 0.72, p-value < 0.01). In contrast, catchments with a $F_{SCA} > \approx 0.38$, aside from NBPV, show a negative statistically significant correlation ($\rho_{Spearman}$ = -0.5, p-value < 0.1). We exclude the NBPV glacier-dominated catchment since its F_{SCA} and F_{yw} relationship is an outlier compared to the other snow-dominated catchments. Note that ERL and ALP catchments are included in both correlations since their F_{SCA} is very close to 0.38. Thus, it is difficult to reliably allocate these catchments to either the "rising" or "falling" limbs of the F_{yw}-F_{SCA} relationship as observable in Fig. 6.

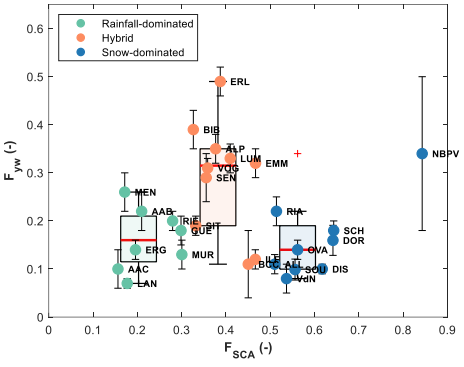

Figure 6. F_{yw} against F_{SCA}. The vertical bars are as in Fig. 4b. The boxplots show the median, quartiles, and whiskers (extending to the most extreme data points not considered outliers, the latter indicated with the '+' red symbol) of the F_{yw} values per regime type, centered on the corresponding median f_{SCA} value per regime type (0.20, 0.38 and 0.56).

4.3.2 The role of quaternary deposits

To advance our understanding of the process that drives F_{yw} according to elevation gradient, we analyze the correlation between the fraction of unconsolidated deposits (F_{qd}) and the young water fraction (Fig. 7), assuming that groundwater is stored in unconsolidated sediments. We exclude the SOU and BCC catchments from our analysis, which show F_{qd} = 0. Considering only the 9 snow-dominated catchments, i.e., the group having the features as close as possible to those used by Arnoux et al. (2021), we find a Spearman rank correlation coefficient of -0.5 with a p-value of 0.22, meaning a negative, but not statistically significant correlation between F_{yw} and F_{qd}. F_{yw} values of the 10 hybrid catchments reveal a positive, but non-significant correlation with unconsolidated sediments ($\rho_{Spearman}$ = 0.4, p-value = 0.29). Finally, rainfall-dominated catchments show a negative, non-significant correlation ($\rho_{Spearman}$ = -0.52, p-value = 0.2).

https://doi.org/10.5194/egusphere-2022-921
Preprint. Discussion started: 20 September 2022

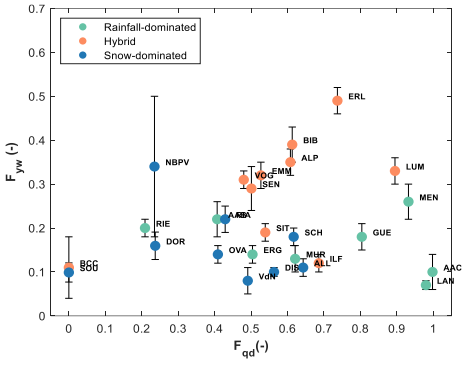

Figure 7. Plot of F_{yw} against the fraction of quaternary deposits (F_{qd})

4.3.3 Groundwater contribution to streamflow: *WFI* and F_{bf} related with F_{yw}

Analysis by Arnoux et al. (2021) revealed that the fraction of quaternary deposits is positively correlated with the low-flow indicators (e.g., *WFI*) in high-elevation catchments. This evidence indicates that catchments with high *WFI* receive an important contribution from groundwater (Arnoux et al., 2021). This is also confirmed by our dataset (Fig. 8a). Indeed, if we look at snow-dominated catchments, always removing the SOU catchment since it shows a F_{qd} = 0, we find a positive and statistically significant correlation ($\rho_{Spearman}$= 0.67 p-value < 0.1) of F_{qd} with the *WFI*. Conversely, we do not find statistically significant correlations for hybrid (negative correlation) and rainfall-dominated (positive correlation) catchments. In exchange, *WFI* is negatively and significantly correlated with the young water fractions of the entire dataset ($\rho_{Spearman}$= -0.40 p-value < 0.1) as shown in Fig. 8b.

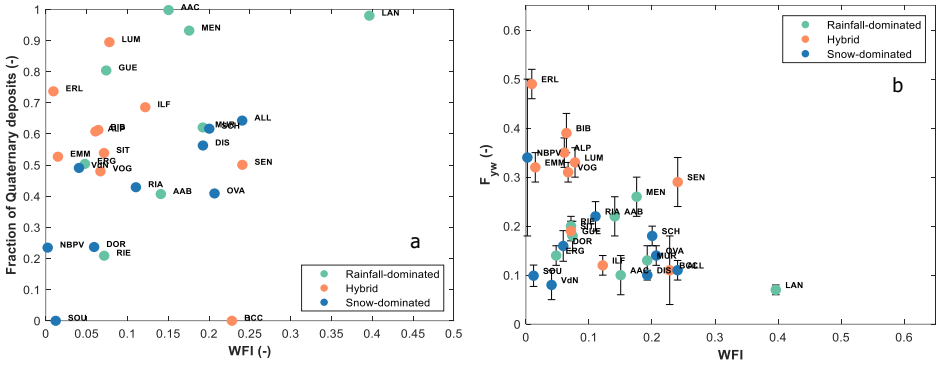

Figure 8. a) Fraction of quaternary deposits plotted against WFI; b) Young water fraction plotted against WFI.

As described in Section 3.5, we apply the baseflow filter of Duncan et al. (2019) to the daily discharge data of the 27 study catchments for having a more physical evaluation of the groundwater contribution to streamflow. The resulting baseflow time series are reported in Fig. 9 for the selected six representative study catchments (time series for all the study sites are available in the Supplementary Material, Fig. S3).

To directly compare the F_{yw} with the amount of baseflow, considered here as a proxy for groundwater, we calculate the average fraction of baseflow (F_{bf}) as reported in Section 3.5. We obtain a strongly negative and significant correlation of F_{yw} with F_{bf} ($\rho_{Spearman}$= -0.75 p-value < 0.01) as shown in Fig. 10. The F_{bf} is generally lower for hybrid catchments (median F_{bf} of 0.67) than for rainfall-dominated catchments (median F_{bf} of 0.74) and snow-dominated catchments (median F_{bf} of

https://doi.org/10.5194/egusphere-2022-921
Preprint. Discussion started: 20 September 2022

0.84). Moreover, the fit of a line of F_{yw} as a function of F_{bf} points (*cftool*, Matlab R2019b) demonstrates a complementary relationship (R^2 = 0.65):

$$F_{yw} = -(0.93 \pm 0.19)F_{bf} + (0.91 \pm 0.22)\,, \quad (9)$$

Interestingly, we find that the NBPV catchment has a lower F_{bf} (≈ 0.7) if compared to the median F_{bf} of catchments belonging to the same regime. All the results in terms of median values per regime are summarized in Table 3. The full results table (Table S1) for all catchments is available in the Supplementary Material.

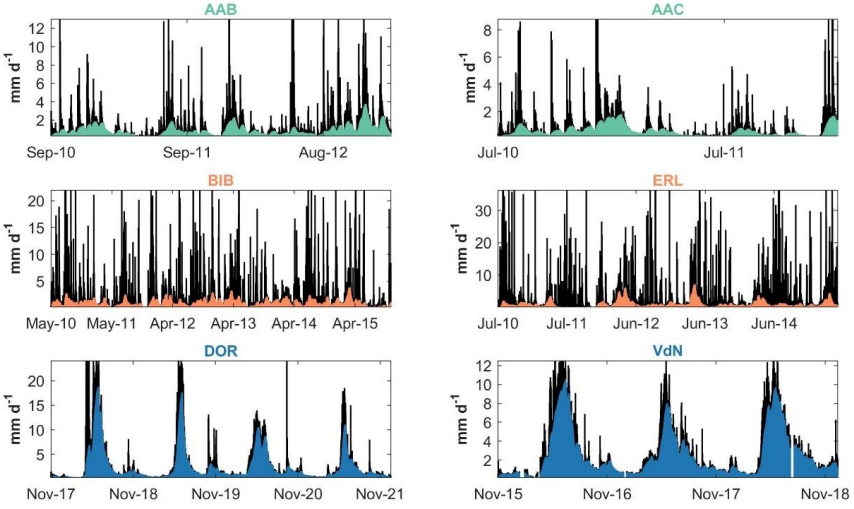

Figure 9. Baseflow separation for six representative study catchments using the Duncan (2019) filter. The black area represents the daily discharge, while the coloured area represents the estimated daily baseflow.

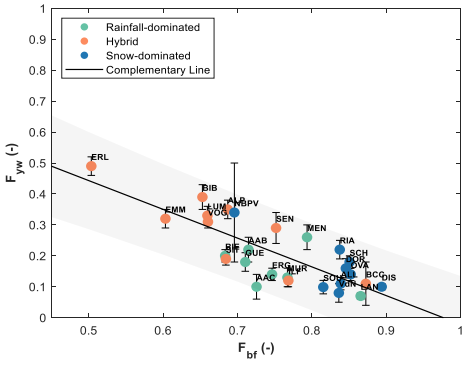

Figure 10. Young water fraction plotted against fraction of baseflow. Grey area represents the 95% prediction bounds of a linear regression of F_{yw} on F_{bf}.

https://doi.org/10.5194/egusphere-2022-921
Preprint. Discussion started: 20 September 2022

Table 3. Summary table with all the results in terms of median values with associated Inter Quartile Range (IQR) for each hydro-climatic regime.

	rainfall-dominated		hybrid		snow-dominated	
	median	IQR	median	IQR	median	IQR
F_{yw} (-)	0.16	0.10	0.32	0.16	0.14	0.09
F_{bf} (-)	0.74	0.07	0.67	0.10	0.84	0.02
WFI (-)	0.15	0.11	0.07	0.06	0.11	0.17
F_{qd} (-)	0.71	0.50	0.57	0.19	0.43	0.34
F_{SCA} (-)	0.20	0.11	0.38	0.09	0.56	0.11
Q_{June}/Q_{DJF} (-)	0.26	0.10	0.47	0.41	3.74	2.95

5 Discussion

5.1 The new hydro-climatic regime classification

For each of the three hydro-climatic regimes, it is possible to define an average characteristic shape of the monthly hydrograph (Fig. 11). A shift of the monthly hydrograph peak of about 1.5 months is observed passing from rainfall-dominated (peak in March) to hybrid catchments (peak in mid-April) and then, passing from a hybrid to a snow-dominated (peak in June) regime (Fig. 11). This "flow peak-shifting" is a clear sign of the increasing predominance of snowmelt in the streamflow generation processes and is at the basis of Pardé-Coefficient based regime classifications. Accordingly, the value of the classification proposed here is not to shed new light on streamflow dynamics but to objectively connect the streamflow regime shape to summer-to-winter streamflow ratios and to the mean snow cover extent. The new classification scheme can be applied outside Switzerland and the objective and explicative classifiers, on which it is based, allow the study of regime changes (e.g., from snow-dominated to hybrid) that will become increasingly more apparent under climate change (Lucianetti et al., 2020; Harrison et al., 2021).

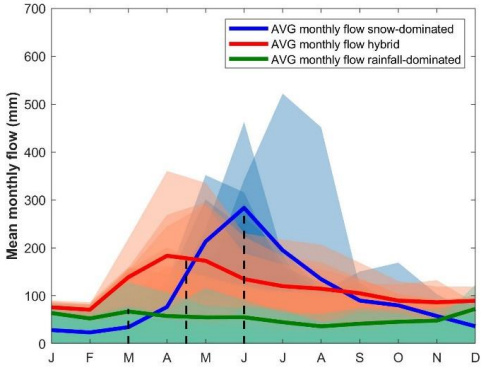

Figure 11. Coloured areas represent the monthly flow of each study catchment. The solid lines indicate the average monthly flow for each hydro-climatic regime, thus defining a characteristic shape of the monthly hydrograph for each of such regimes. Dashed black lines show the month in which, on average, the peak-flow is observed for each hydro-climatic regime.

https://doi.org/10.5194/egusphere-2022-921
Preprint. Discussion started: 20 September 2022

5.2 A perceptual model: snowpack persistency favours increasing water age.

A perceptual model that describes the theoretical behavior of young water fraction with varying F_{SCA} emerges from our analysis and harmonizes the results of this work with that of previous studies.

A plot of F_{SCA} against F_{yw} (Fig. 12a) shows a bell-shaped behavior (which we visualize with the grey shade in Fig. 12a) that suggests the interplay of two different trends: a positive trend as long as $F_{SCA} < \approx 0.38$ and a negative trend for $F_{SCA} > \approx 0.38$. This threshold (that is the median f_{SCA} of hybrid catchments) splits the hybrid regime in two sub-classes.

The first sub-class (elevation $< \approx$1500 m a.s.l.) is mainly influenced by the rain-dominated regime. Accordingly, the rising limb of the bell-shaped curve can be primarily explained by the increase of precipitation and slope with elevation (Fig. 12a, Fig. 4a) and the reduction of evaporation with elevation due to reduced temperatures (Goulden et al., 2012). As elevation increases, these factors favor an ever-growing lateral and longitudinal connectivity (Tromp-van Meerveld and McDonnell, 2006; McDonnell, 2013; McDonnell et al., 2021) producing wetness conditions that promote rapid flow paths: the young water fraction increases but also groundwater recharge; this promotion of groundwater recharge is visible in a plot of winter baseflow against elevation (Fig. S4). In addition, higher order channels, higher up, are more rarely activated than lower order channels that are more often active (Botter et al., 2021; Durighetto et al., 2022). Therefore, it is more likely that lower order channels are draining more old water than the temporary activated higher order channels: water age decreases with elevation when catchments reveal a negligible or a shallow, possibly ephemeral, snowpack. In fact, the limited number of snowfall days and mid-winter melt reduce the snow accumulation in the lower elevation sub-class of hybrid regimes. Such a snowpack does not protect the underlying soils from freezing (Harrison et al., 2021). Even for low elevation locations ($< \approx$1500 m asl.), freezing conditions are regularly observed during winter (Keller et al., 2017): such conditions can lead to soil freezing thereby inhibiting infiltration and favoring rapid flow paths during mid-winter melt events, with subsequent increase of F_{yw}.

In contrast, the second sub-class (elevation $> \approx$1500 m a.s.l.) of hybrid catchments is increasingly influenced by the snow-regime. Here, the building up of a persistent, deep snowpack can promote deep vertical infiltration by insulating the soil and thereby preventing freezing (Jasechko et al., 2016; Harrison et al., 2021). The resulting effect on water partitioning between the surface and the subsurface has however to be analyzed in light of the temporal concentration of water input on the snowmelt period and remains largely unexplored to date (Rey et al., 2021). Despite of this, the temporal dynamic of snow accumulation and melt and its effect on deep infiltration supports the pivotal role of snowmelt in recharging groundwater during summer in high-elevation environments (Flerchinger et al., 1992; Cochand et al., 2019; Du et al., 2019). Moreover, the analysis of Lucianetti et al. (2020) revealed different varying proportions of rain and snow contributions to the recharge of springs in the Dolomites according to elevations. Specifically, they observed a gradually higher snowmelt contribution in springs passing from roughly 46% below 2000 m a.s.l to nearly 72% above 2500 m a.s.l.

To advance our understanding of F_{yw} along elevation gradients, we also need to ask how and when groundwater storage contributes to streamflow. Here, another crucial function of the seasonal snowpack comes into play: it favors the emptying of the groundwater storage over long winter recession periods. In some snow-dominated environments, the seasonal snow cover can persist for more than six months, and the streams correspondingly show a low-flow regime resulting from absence of rain and melt input, with minimum flow during winter decreasing below 0.5 to 1 mm/d for the highest locations (Fig. S5). It is assumed that these low-flow periods, generally consistent from year to year because of the annual temperature cycle, are sustained by the groundwater storage that provides resilience to Alpine rivers (Hayashi, 2020). This groundwater (or old water) contribution to streamflow during the winter period increases the age of streamwater. In addition, high elevation catchments can reveal winter low-flow periods that are significantly longer than their high-flow

https://doi.org/10.5194/egusphere-2022-921
Preprint. Discussion started: 20 September 2022

periods (Hayashi, 2020). In conclusion, this low-flow period could strongly influence the water age, thereby decreasing the F_{yw}.

The above mechanisms are summarized in the perceptual model reported in Fig. 13 also indicating which are the dominant processes over the winter and summer seasons. This model is, however, not able to explain the NBPV catchment hydrological functioning, which is classified as snow-dominated according to our classification criterion, but our criterion does not consider the influence of glaciers. The NBPV catchment area is 42% glacier covered, so it is probable that this catchment should belong to a fourth class of "glacier-dominated" catchments (in fact, it is detected as an outlier: see blue boxplot in Fig. 12a). Such catchments could show fast flow paths and small storages as e.g. discussed in the work of Jansson et al. (2003), reviewing glacier-dominated environments. Moreover, reduced baseflow during winter can be related to increasingly high temperatures causing the glaciers retreat, thus reducing and anticipating the glacier melt fluxes that possibly recharge groundwater (Hayashi, 2020).

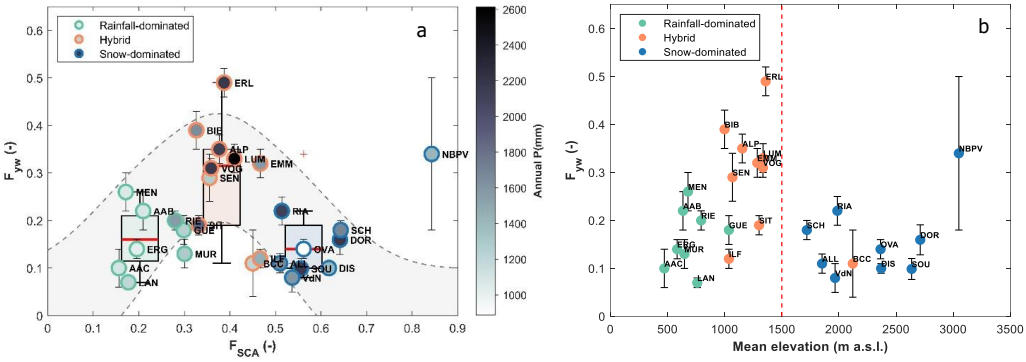

Figure 12. a) Theoretical behavior of young water fraction with varying F_{SCA} indicated by the grey area b) F_{yw} as function of mean catchment elevation. The dashed red line indicates the threshold elevation above which the F_{yw}-reset is observed.

5.3 The role of unconsolidated sediments in increasing or decreasing water age

We have achieved correlation that is not statistically significant between F_{qd} and F_{yw} that can be explained considering that unconsolidated sediments are not the only groundwater storage contribution to the stream during low-flow periods in such environments. In steeper catchments, additional storage is provided by the bedrock fractures (Gleeson et al., 2014; Jasechko et al., 2016; Martin et al., 2021) and by the bedrock geology which has influence on groundwater retention capacity (Hayashi, 2020). However, necessary data is elusive.

The positive correlation between F_{yw} and F_{qd} in hybrid catchments can be explained by two mechanisms: i) high baseflow points towards system saturation being high, which favors connectivity and ii) ephemeral snowpacks can favor freezing phenomena inhibiting winter snowmelt infiltration and thereby favoring fast flow processes (Harrison et al., 2021). Concluding, we stress that more catchments and more geological information would be required to statistically validate these observations.

https://doi.org/10.5194/egusphere-2022-921
Preprint. Discussion started: 20 September 2022

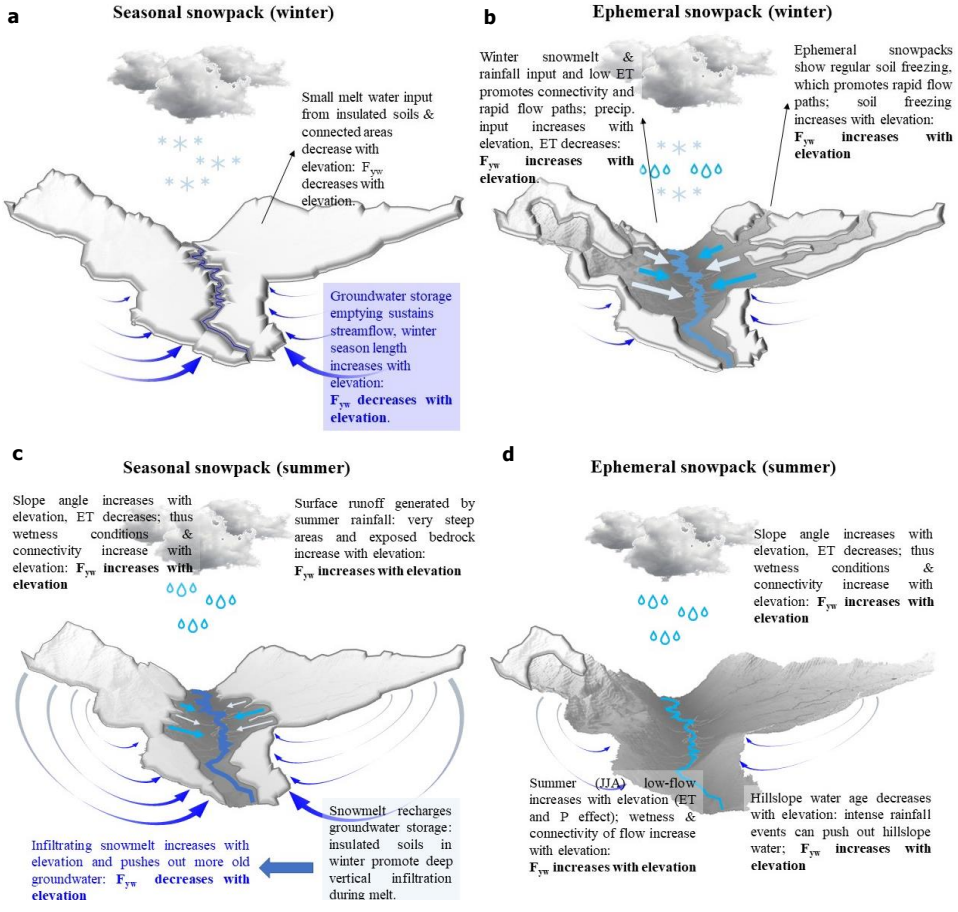

Figure 13. Perceptual model of different hydrological functioning of catchments characterized by ephemeral snowpacks, in panels b (winter) and d (summer), and by seasonal snowpacks, panels a (winter) and c (summer).

5.4 Groundwater contribution to streamflow is the key to understand F_{yw} gradients

We have tested here if the counterintuitive low F_{yw} obtained for high-elevation catchments depends on the groundwater contribution to streamflow and if the results are consistent with our perceptual model. We obtain a statistically significant negative correlation between F_{yw} and F_{bf} (Fig. 10) and the linear fit of the points suggests that F_{bf} is roughly the one's complement of F_{yw}. This result clearly indicates that the observed patterns of F_{yw} are related to water partitioning between the surface and the subsurface. Moreover, this complementarity gives a further physical meaning for the estimated baseflow in our data set: the estimated baseflow should correspond to water with transit times higher than roughly 0.2 years.

We find the highest F_{bf} for snow-dominated catchments confirming the presence of high subsurface storage, contributing to streams, in high-elevation catchments (Staudinger et al., 2017). Moreover, the annual baseflow is strongly positively correlated with the F_{SCA} ($\rho_{Spearman}$= 0.81 p-value < 0.01) suggesting a major groundwater contribution with increasing snow cover persistency (Fig. S6).

https://doi.org/10.5194/egusphere-2022-921
Preprint. Discussion started: 20 September 2022

The major dispersion of F_{bf} we find in hybrid catchments supports the idea that such catchments can reveal a different hydrological functioning depending on whether they are mainly influenced by the rain or snow regime. The hydro-climatic regime is generally a good indicator of the proportion of young water that contributes to streamflow, with a few exceptions though. Interestingly, the F_{bf} offers an explanation for these exceptions. For example, the BCC catchment is classified as hybrid, but it reveals a low F_{yw} (0.11) that is comparable with those obtained for snow-dominated catchments (median F_{yw} = 0.14). In fact, BCC reveals a F_{SCA} of 0.45, very close to the threshold of 0.5 for being classified as snow-dominated (Table 2) and a high F_{bf} (0.87) underlining the dominant role of groundwater in the streamflow generation. This result is consistent with previous findings of Penna et al. (2016) for this catchment: they have shown that, on average, from 80% to 98% of BCC discharge is constituted by pre-event water (assumed to represent groundwater).

Another special case is the NBPV catchment: it is an outlier in the F_{yw}-F_{SCA} space (Fig. 12a, i.e., the perceptual model is not able to explain its high F_{yw}) but it results to be in line with the other catchments in the F_{yw}-F_{bf} space (Fig. 10) and its relatively high F_{yw} (0.34) can reasonably be explained with a relatively low F_{bf} (0.70, i.e. a relatively low groundwater contribution to streamflow).

Therefore, we can conclude that the contribution of groundwater storage to streamflow, which is driven by snowpack duration, can be considered as the best explanatory variable of the F_{yw} elevation gradients.

6 Conclusion

This paper demonstrates, based on a new collection of observations of high-elevation catchments from both published datasets and new field observations, that Alpine young water fractions, F_{yw}, show a topographic pattern that is characterized with an increase to about 1500 m a.s.l., and a decrease thereafter. We provide here an explanation for this pattern, thereby clarifying why F_{yw} is low in high-elevation catchments, filling a knowledge gap expressed in previous studies. All the study catchments have been classified in three categories: rainfall-dominated, hybrid or snow-dominated. We do this through a new classification scheme that can be applied using objective and parsimonious classifiers: the summer/winter discharge ratio (Q_{June}/Q_{DJF}) and the fractional snow cover area (F_{SCA}). These classifiers strongly correlate; therefore, it is possible to use the easy to calculate Q_{June}/Q_{DJF} for obtaining a first order estimate of F_{SCA} through the exponential relationship proposed in this paper.

We focus on the correlations between F_{yw} and three selected variables: the fraction of quaternary deposits, F_{qd}, F_{SCA}, and the fraction of baseflow, F_{bf}. Additionally, we consider the Winter Flow Index (*WFI*) for comparing our results about the groundwater contribution to streamflow with those of previous works.

The fraction of quaternary deposits (F_{qd}), assumed to store groundwater, does not produce a statistically significant correlation with F_{yw}; however, this analysis should be completed with more detailed geological information, e.g., the bedrock geology or the fraction of fractured bedrock, which is hard to retrieve in geological data set.

The relationship between F_{yw} and F_{SCA} shows a bell-shaped curve that suggests the activation of different hydrological processes depending on the snowpack duration (ranging from ephemeral to seasonal). Building from this observation, we develop a perceptual model of how snow persistency explains F_{yw} during winter and summer along topographic gradients: during winter, at elevations with an ephemeral snowpack ($< \approx$ 1500 m a.s.l.), high system wetness and soil freezing favor rapid flow paths leading to high F_{yw}; at elevations with a seasonal snowpack ($> \approx$ 1500 m a.s.l.), there is almost no water input during winter and streamflow is fed by progressively emptying groundwater storage, leading to low F_{yw}. These seasonal snowpacks insulate soils, thereby promoting deep vertical infiltration on the snowmelt onset and supporting the pivotal role of snowmelt in recharging groundwater storage in high mountain environments during summer. This recharge

https://doi.org/10.5194/egusphere-2022-921
Preprint. Discussion started: 20 September 2022

leads to high baseflow throughout the year, especially during winter, and only few streamflow events characterized by fast flow paths. Since winter low-flow periods can be longer than high-flow periods in snow-dominated catchments, such periods influence the water age at annual scale and thereby lead to decreasing F_{yw} with winter duration (i.e., with elevation).

This perceptual model is corroborated by the high negative correlation between F_{bf} and F_{yw}, which indicates a key-role of groundwater in streamflow generation processes and further confirmed by the negative and significant correlation between *WFI* and F_{yw}. Nevertheless, our model is not able to explain the hydrological functioning of the single glacier-dominated catchment in our dataset, even if we can explain its high F_{yw} by the relatively low groundwater contribution (i.e., low F_{bf}). Thus, further research is necessary to conceptualize the processes of such systems that under glacier retreat will see a gradual transition to purely snow-dominated systems.

Data availability. DOR and SOU data are available from Alessio Gentile upon reasonable request. Data of the remaining 25 catchments are freely available online and all the data sources are cited in the manuscript.

Supplement. The supplement related to this article is available online at

Author contributions. AG, NC, BS and SF identified the research gap, defined the methodology, developed the perceptual model, and prepared the paper. AG analyzed the data set. DG, DC, MP and SF collected the water samples for the DOR and SOU catchments. GZ analyzed spatial data related to NBPV and BCC catchments. All authors revised the manuscript and gave final approval to the submitted version.

Competing interests. The authors declare that they have no conflict of interest.

Acknowledgements. This work was supported by the *"PRIN MIUR 2017SL7ABC_005 WATZON Project"* and the *"MIUR - Excellence Department: National funds allocated to the DIST department"*. We warmly thank the *"COST Action CA19120 - WATSON (WATer isotopeS in the critical zONe)"* for the acceptance of the application procedure for one Virtual Mobility (VM) and one Short Term Scientific Mission (STSM). Both activities allowed to speed up the planning and conceptualization of this work as well as to stimulate the collaboration, the sharing of data and ideas. Last but not least, we acknowledge the support of the Valsavarenche Municipality and the Gran Paradiso National Park.

7 References

Aalstad, K., Westermann, S., and Bertino, L.: Evaluating satellite retrieved fractional snow-covered area at a high-Arctic site using terrestrial photography, Remote Sens. Environ., 239, 111618, https://doi.org/10.1016/j.rse.2019.111618, 2020.

Addor, N., Rössler, O., Köplin, N., Huss, M., Weingartner, R., and Seibert, J.: Robust changes and sources of uncertainty in the projected hydrological regimes of Swiss catchments, Water Resour. Res., 50, 7541–7562, https://doi.org/10.1002/2014WR015549, 2014.

Andermann, C., Longuevergne, L., Bonnet, S., Crave, A., Davy, P., and Gloaguen, R.: Impact of transient groundwater storage on the discharge of Himalayan rivers, Nat. Geosci., 5, 127–132, https://doi.org/10.1038/ngeo1356, 2012.

https://doi.org/10.5194/egusphere-2022-921
Preprint. Discussion started: 20 September 2022

Antoniazza, G., Nicollier, T., Boss, S., Mettra, F., Badoux, A., Schaefli, B., Rickenmann, D., and Lane, S. N.: Hydrological Drivers of Bedload Transport in an Alpine Watershed, Water Resour. Res., 58, e2021WR030663, https://doi.org/10.1029/2021WR030663, 2022.

Arnoux, M., Brunner, P., Schaefli, B., Mott, R., Cochand, F., and Hunkeler, D.: Low-flow behavior of alpine catchments with varying quaternary cover under current and future climatic conditions, J. Hydrol., 592, 125591, https://doi.org/10.1016/j.jhydrol.2020.125591, 2021.

Baraer, M., McKenzie, J. M., Mark, B. G., Bury, J., and Knox, S.: Characterizing contributions of glacier melt and groundwater during the dry season in a poorly gauged catchment of the Cordillera Blanca (Peru), in: Advances in Geosciences, 4th EGU Alexander von Humboldt Conference "The Andes: Challenge for Geosciences" - 4th Alexander von Humboldt International Conference on The Andes: Challenge for Geosciences, Santiago de Chile, Chile; 28 November 2008, 41–49, https://doi.org/10.5194/adgeo-22-41-2009, 2009.

Baraer, M., McKenzie, J., Mark, B. G., Gordon, R., Bury, J., Condom, T., Gomez, J., Knox, S., and Fortner, S. K.: Contribution of groundwater to the outflow from ungauged glacierized catchments: a multi-site study in the tropical Cordillera Blanca, Peru, Hydrol. Process., 29, 2561–2581, https://doi.org/10.1002/hyp.10386, 2015.

Benettin, P., Bailey, S. W., Rinaldo, A., Likens, G. E., McGuire, K. J., and Botter, G.: Young runoff fractions control streamwater age and solute concentration dynamics, Hydrol. Process., 31, 2982–2986, https://doi.org/10.1002/hyp.11243, 2017.

Blöschl, G., Bierkens, M. F. P., Chambel, A., Cudennec, C., Destouni, G., Fiori, A., Kirchner, J. W., McDonnell, J. J., Savenije, H. H. G., Sivapalan, M., Stumpp, C., Toth, E., Volpi, E., Carr, G., Lupton, C., Salinas, J., Széles, B., Viglione, A., Aksoy, H., Allen, S. T., Amin, A., Andréassian, V., Arheimer, B., Aryal, S. K., Baker, V., Bardsley, E., Barendrecht, M. H., Bartosova, A., Batelaan, O., Berghuijs, W. R., Beven, K., Blume, T., Bogaard, T., Borges de Amorim, P., Böttcher, M. E., Boulet, G., Breinl, K., Brilly, M., Brocca, L., Buytaert, W., Castellarin, A., Castelletti, A., Chen, X., Chen, Y., Chen, Y., Chifflard, P., Claps, P., Clark, M. P., Collins, A. L., Croke, B., Dathe, A., David, P. C., de Barros, F. P. J., de Rooij, G., Di Baldassarre, G., Driscoll, J. M., Duethmann, D., Dwivedi, R., Eris, E., Farmer, W. H., Feiccabrino, J., Ferguson, G., Ferrari, E., Ferraris, S., Fersch, B., Finger, D., Foglia, L., Fowler, K., Gartsman, B., Gascoin, S., Gaume, E., Gelfan, A., Geris, J., Gharari, S., Gleeson, T., Glendell, M., Gonzalez Bevacqua, A., González-Dugo, M. P., Grimaldi, S., Gupta, A. B., Guse, B., Han, D., Hannah, D., Harpold, A., Haun, S., Heal, K., Helfricht, K., Herrnegger, M., Hipsey, M., Hlaváčiková, H., Hohmann, C., Holko, L., Hopkinson, C., Hrachowitz, M., Illangasekare, T. H., Inam, A., Innocente, C., Istanbulluoglu, E., Jarihani, B., et al.: Twenty-three unsolved problems in hydrology (UPH) – a community perspective, Hydrol. Sci. J., 64, 1141–1158, https://doi.org/10.1080/02626667.2019.1620507, 2019.

Botter, G., Vingiani, F., Senatore, A., Jensen, C., Weiler, M., McGuire, K., Mendicino, G., and Durighetto, N.: Hierarchical climate-driven dynamics of the active channel length in temporary streams, Sci. Rep., 11, 21503, https://doi.org/10.1038/s41598-021-00922-2, 2021.

Carroll, R. W. H., Bearup, L. A., Brown, W., Dong, W., Bill, M., and Willlams, K. H.: Factors controlling seasonal groundwater and solute flux from snow-dominated basins, Hydrol. Process., 32, 2187–2202, https://doi.org/10.1002/hyp.13151, 2018.

Carturan, L.: Replacing monitored glaciers undergoing extinction: a new measurement series on La Mare Glacier (Ortles-Cevedale, Italy), J. Glaciol., 62, 1093–1103, https://doi.org/10.1017/jog.2016.107, 2016.

Carturan, L., Baroni, C., Becker, M., Bellin, A., Cainelli, O., Carton, A., Casarotto, C., Dalla Fontana, G., Godio, A., Martinelli, T., Salvatore, M. C., and Seppi, R.: Decay of a long-term monitored glacier: Careser Glacier (Ortles-Cevedale, European Alps), The Cryosphere, 7, 1819–1838, https://doi.org/10.5194/tc-7-1819-2013, 2013.

https://doi.org/10.5194/egusphere-2022-921
Preprint. Discussion started: 20 September 2022

Carturan, L., Baroni, C., Carton, A., Cazorzi, F., Fontana, G. D., Delpero, C., Salvatore, M. C., Seppi, R., and Zanoner, T.: Reconstructing fluctuations of la mare glacier (eastern italian alps) in the late holocene: new evidence for a little ice age maximum around 1600 ad, Geogr. Ann. Ser. Phys. Geogr., 96, 287–306, https://doi.org/10.1111/geoa.12048, 2014.

Carturan, L., Zuecco, G., Seppi, R., Zanoner, T., Borga, M., Carton, A., and Dalla Fontana, G.: Catchment-Scale Permafrost Mapping using Spring Water Characteristics, Permafr. Periglac. Process., 27, 253–270, https://doi.org/10.1002/ppp.1875, 2016.

Carturan, L., De Blasi, F., Cazorzi, F., Zoccatelli, D., Bonato, P., Borga, M., and Dalla Fontana, G.: Relevance and Scale Dependence of Hydrological Changes in Glacierized Catchments: Insights from Historical Data Series in the Eastern Italian Alps, Water, 11, 89, https://doi.org/10.3390/w11010089, 2019.

Ceperley, N., Zuecco, G., Beria, H., Carturan, L., Michelon, A., Penna, D., Larsen, J., and Schaefli, B.: Seasonal snow cover decreases young water fractions in high Alpine catchments, Hydrol. Process., 34, 4794–4813, https://doi.org/10.1002/hyp.13937, 2020.

Chen, Z., Hartmann, A., Wagener, T., and Goldscheider, N.: Dynamics of water fluxes and storages in an Alpine karst catchment under current and potential future climate conditions, Hydrol. Earth Syst. Sci., 22, 3807–3823, https://doi.org/10.5194/hess-22-3807-2018, 2018.

Christensen, C. W., Hayashi, M., and Bentley, L. R.: Hydrogeological characterization of an alpine aquifer system in the Canadian Rocky Mountains, Hydrogeol. J., 28, 1871–1890, https://doi.org/10.1007/s10040-020-02153-7, 2020.

Clow, D. w., Schrott, L., Webb, R., Campbell, D. h., Torizzo, A., and Dornblaser, M.: Ground Water Occurrence and Contributions to Streamflow in an Alpine Catchment, Colorado Front Range, Groundwater, 41, 937–950, https://doi.org/10.1111/j.1745-6584.2003.tb02436.x, 2003.

Cochand, M., Christe, P., Ornstein, P., and Hunkeler, D.: Groundwater Storage in High Alpine Catchments and Its Contribution to Streamflow, Water Resour. Res., 55, 2613–2630, https://doi.org/10.1029/2018WR022989, 2019.

Cowie, R. M., Knowles, J. F., Dailey, K. R., Williams, M. W., Mills, T. J., and Molotch, N. P.: Sources of streamflow along a headwater catchment elevational gradient, J. Hydrol., 549, 163–178, https://doi.org/10.1016/j.jhydrol.2017.03.044, 2017.

Curran, J. H. and Biles, F. E.: Identification of Seasonal Streamflow Regimes and Streamflow Drivers for Daily and Peak Flows in Alaska, Water Resour. Res., 57, e2020WR028425, https://doi.org/10.1029/2020WR028425, 2021.

Déry, S. J., Stahl, K., Moore, R. D., Whitfield, P. H., Menounos, B., and Burford, J. E.: Detection of runoff timing changes in pluvial, nival, and glacial rivers of western Canada, Water Resour. Res., 45, https://doi.org/10.1029/2008WR006975, 2009.

Di Marco, N., Righetti, M., Avesani, D., Zaramella, M., Notarnicola, C., and Borga, M.: Comparison of MODIS and Model-Derived Snow-Covered Areas: Impact of Land Use and Solar Illumination Conditions, 20, 2020.

Dozier, J.: Spectral signature of alpine snow cover from the landsat thematic mapper, Remote Sens. Environ., 28, 9–22, https://doi.org/10.1016/0034-4257(89)90101-6, 1989.

Duncan, H. P.: Baseflow separation – A practical approach, J. Hydrol., 575, 308–313, https://doi.org/10.1016/j.jhydrol.2019.05.040, 2019.

Durighetto, N., Mariotto, V., Zanetti, F., McGuire, K. J., Mendicino, G., Senatore, A., and Botter, G.: Probabilistic Description of Streamflow and Active Length Regimes in Rivers, Water Resour. Res., 58, e2021WR031344, https://doi.org/10.1029/2021WR031344, 2022.

https://doi.org/10.5194/egusphere-2022-921
Preprint. Discussion started: 20 September 2022

Engel, M., Penna, D., Bertoldi, G., Dell'Agnese, A., Soulsby, C., and Comiti, F.: Identifying run-off contributions during melt-induced run-off events in a glacierized alpine catchment, Hydrol. Process., 30, 343–364, https://doi.org/10.1002/hyp.10577, 2016.

von Freyberg, J., Allen, S. T., Seeger, S., Weiler, M., and Kirchner, J. W.: Sensitivity of young water fractions to hydro-climatic forcing and landscape properties across 22 Swiss catchments, Hydrol. Earth Syst. Sci., 22, 3841–3861, https://doi.org/10.5194/hess-22-3841-2018, 2018.

von Freyberg, J., Rücker, A., Zappa, M., Schlumpf, A., Studer, B., and Kirchner, J. W.: Four years of daily stable water isotope data in stream water and precipitation from three Swiss catchments, Sci. Data, 9, 46, https://doi.org/10.1038/s41597-022-01148-1, 2022.

Frisbee, M. D., Phillips, F. M., Campbell, A. R., Liu, F., and Sanchez, S. A.: Streamflow generation in a large, alpine watershed in the southern Rocky Mountains of Colorado: Is streamflow generation simply the aggregation of hillslope runoff responses?, Water Resour. Res., 47, https://doi.org/10.1029/2010WR009391, 2011.

Gallart, F., Valiente, M., Llorens, P., Cayuela, C., Sprenger, M., and Latron, J.: Investigating young water fractions in a small Mediterranean mountain catchment: Both precipitation forcing and sampling frequency matter, Hydrol. Process., 34, 3618–3634, https://doi.org/10.1002/hyp.13806, 2020.

Gascoin, S., Grizonnet, M., Bouchet, M., Salgues, G., and Hagolle, O.: Theia Snow collection: high-resolution operational snow cover maps from Sentinel-2 and Landsat-8 data, Earth Syst. Sci. Data, 11, 493–514, https://doi.org/10.5194/essd-11-493-2019, 2019.

Gisolo, D., Previati, M., Bevilacqua, I., Canone, D., Boetti, M., Dematteis, N., Balocco, J., Ferrari, S., Gentile, A., Nsassila, M., Heery, B., Vereecken, H., and Ferraris, S.: A Calibration Free Radiation Driven Model for Estimating Actual Evapotranspiration of Mountain Grasslands (CLIME-MG), J. Hydrol., 127948, https://doi.org/10.1016/j.jhydrol.2022.127948, 2022.

Gleeson, T. and Manning, A. H.: Regional groundwater flow in mountainous terrain: Three-dimensional simulations of topographic and hydrogeologic controls, Water Resour. Res., 44, https://doi.org/10.1029/2008WR006848, 2008.

Gleeson, T., Moosdorf, N., Hartmann, J., and van Beek, L. P. H.: A glimpse beneath earth's surface: GLobal HYdrogeology MaPS (GLHYMPS) of permeability and porosity, Geophys. Res. Lett., 41, 3891–3898, https://doi.org/10.1002/2014GL059856, 2014.

Gordon, R. P., Lautz, L. K., McKenzie, J. M., Mark, B. G., Chavez, D., and Baraer, M.: Sources and pathways of stream generation in tropical proglacial valleys of the Cordillera Blanca, Peru, J. Hydrol., 522, 628–644, https://doi.org/10.1016/j.jhydrol.2015.01.013, 2015.

Goulden, M. L., Anderson, R. G., Bales, R. C., Kelly, A. E., Meadows, M., and Winston, G. C.: Evapotranspiration along an elevation gradient in California's Sierra Nevada, J. Geophys. Res. Biogeosciences, 117, https://doi.org/10.1029/2012JG002027, 2012.

Guastini, E., Zuecco, G., Errico, A., Castelli, G., Bresci, E., Preti, F., and Penna, D.: How does streamflow response vary with spatial scale? Analysis of controls in three nested Alpine catchments, J. Hydrol., 570, 705–718, https://doi.org/10.1016/j.jhydrol.2019.01.022, 2019.

Hall, F. R.: Base-Flow Recessions—A Review, Water Resour. Res., 4, 973–983, https://doi.org/10.1029/WR004i005p00973, 1968.

Harrington, J. S., Mozil, A., Hayashi, M., and Bentley, L. R.: Groundwater flow and storage processes in an inactive rock glacier, Hydrol. Process., 32, 3070–3088, https://doi.org/10.1002/hyp.13248, 2018.

https://doi.org/10.5194/egusphere-2022-921
Preprint. Discussion started: 20 September 2022

Harrison, H. N., Hammond, J. C., Kampf, S., and Kiewiet, L.: On the hydrological difference between catchments above and below the intermittent-persistent snow transition, Hydrol. Process., 35, e14411, https://doi.org/10.1002/hyp.14411, 2021.

Hayashi, M.: Alpine Hydrogeology: The Critical Role of Groundwater in Sourcing the Headwaters of the World, Ground Water, 58, 498–510, https://doi.org/10.1111/gwat.12965, 2020.

Hofmeister, F., Arias-Rodriguez, L. F., Premier, V., Marin, C., Notarnicola, C., Disse, M., and Chiogna, G.: Intercomparison of Sentinel-2 and modelled snow cover maps in a high-elevation Alpine catchment, J. Hydrol. X, 15, 100123, https://doi.org/10.1016/j.hydroa.2022.100123, 2022.

Jasechko, S.: Global Isotope Hydrogeology—Review, Rev. Geophys., 57, 835–965, https://doi.org/10.1029/2018RG000627, 2019.

Jasechko, S., Kirchner, J. W., Welker, J. M., and McDonnell, J. J.: Substantial proportion of global streamflow less than three months old, Nat. Geosci., 9, 126–129, https://doi.org/10.1038/ngeo2636, 2016.

Jenicek, M., Seibert, J., and Staudinger, M.: Modeling of Future Changes in Seasonal Snowpack and Impacts on Summer Low Flows in Alpine Catchments, Water Resour. Res., 54, 538–556, https://doi.org/10.1002/2017WR021648, 2018.

Käser, D. and Hunkeler, D.: Contribution of alluvial groundwater to the outflow of mountainous catchments, Water Resour. Res., 52, 680–697, https://doi.org/10.1002/2014WR016730, 2016.

Keller, D. E., Fischer, A. M., Liniger, M. A., Appenzeller, C., and Knutti, R.: Testing a weather generator for downscaling climate change projections over Switzerland, Int. J. Climatol., 37, 928–942, https://doi.org/10.1002/joc.4750, 2017.

Kirchner, J. W.: A double paradox in catchment hydrology and geochemistry, Hydrol. Process., 17, 871–874, https://doi.org/10.1002/hyp.5108, 2003.

Kirchner, J. W.: Aggregation in environmental systems-Part 1: Seasonal tracer cycles quantify young water fractions, but not mean transit times, in spatially heterogeneous catchments, Hydrol. Earth Syst. Sci., 20, 279–297, https://doi.org/10.5194/hess-20-279-2016, 2016a.

Kirchner, J. W.: Aggregation in environmental systems-Part 2: Catchment mean transit times and young water fractions under hydrologic nonstationarity, Hydrol. Earth Syst. Sci., 20, 299–328, https://doi.org/10.5194/hess-20-299-2016, 2016b.

Liu, F., Williams, M. W., and Caine, N.: Source waters and flow paths in an alpine catchment, Colorado Front Range, United States, Water Resour. Res., 40, https://doi.org/10.1029/2004WR003076, 2004.

Lucianetti, G., Penna, D., Mastrorillo, L., and Mazza, R.: The Role of Snowmelt on the Spatio-Temporal Variability of Spring Recharge in a Dolomitic Mountain Group, Italian Alps, Water, 12, 2256, https://doi.org/10.3390/w12082256, 2020.

Lutz, S. R., Krieg, R., Müller, C., Zink, M., Knöller, K., Samaniego, L., and Merz, R.: Spatial Patterns of Water Age: Using Young Water Fractions to Improve the Characterization of Transit Times in Contrasting Catchments, Water Resour. Res., 54, 4767–4784, https://doi.org/10.1029/2017WR022216, 2018.

Martin, C., Kampf, S. K., Hammond, J. C., Wilson, C., and Anderson, S. P.: Controls on Streamflow Densities in Semiarid Rocky Mountain Catchments, Water, 13, 521, https://doi.org/10.3390/w13040521, 2021.

Martinec, J.: Subsurface flow from snowmelt traced by tritium, Water Resour. Res., 11, 496–498, https://doi.org/10.1029/WR011i003p00496, 1975.

McDonnell, J. J.: Are all runoff processes the same?, Hydrol. Process., 27, 4103–4111, https://doi.org/10.1002/hyp.10076, 2013.

McDonnell, J. J.: Beyond the water balance, Nat. Geosci., 10, 396–396, https://doi.org/10.1038/ngeo2964, 2017.

https://doi.org/10.5194/egusphere-2022-921
Preprint. Discussion started: 20 September 2022

McDonnell, J. J., Spence, C., Karran, D. J., van Meerveld, H. J. (Ilja), and Harman, C. J.: Fill-and-Spill: A Process Description of Runoff Generation at the Scale of the Beholder, Water Resour. Res., 57, e2020WR027514, https://doi.org/10.1029/2020WR027514, 2021.

Michelon, A., Ceperley, N., Beria, H., Larsen, J., Vennemann, T., and Schaefli, B.: Studying the dynamic of a high alpine catchment based on multiple natural tracers, Hydrol. Earth Syst. Sci. Discuss., 1–43, https://doi.org/10.5194/hess-2022-48, 2022.

Moore, R. D. (Dan), Trubilowicz, J. w., and Buttle, J. m: Prediction of Streamflow Regime and Annual Runoff for Ungauged Basins Using a Distributed Monthly Water Balance Model1, JAWRA J. Am. Water Resour. Assoc., 48, 32–42, https://doi.org/10.1111/j.1752-1688.2011.00595.x, 2012.

Pardè, M.: Fleuves et rivières, Librairie Armand Colin, Paris, 1933.

Paznekas, A. and Hayashi, M.: Groundwater contribution to winter streamflow in the Canadian Rockies, Can. Water Resour. J. Rev. Can. Ressour. Hydr., 41, 484–499, https://doi.org/10.1080/07011784.2015.1060870, 2016.

Penna, D., van Meerveld, H. J., Zuecco, G., Dalla Fontana, G., and Borga, M.: Hydrological response of an Alpine catchment to rainfall and snowmelt events, J. Hydrol., 537, 382–397, https://doi.org/10.1016/j.jhydrol.2016.03.040, 2016.

Penna, D., Engel, M., Bertoldi, G., and Comiti, F.: Towards a tracer-based conceptualization of meltwater dynamics and streamflow response in a glacierized catchment, Hydrol. Earth Syst. Sci., 21, 23–41, https://doi.org/10.5194/hess-21-23-2017, 2017.

Petersky, R. and Harpold, A.: Now you see it, now you don't: a case study of ephemeral snowpacks and soil moisture response in the Great Basin, USA, Hydrol. Earth Syst. Sci., 22, 4891–4906, https://doi.org/10.5194/hess-22-4891-2018, 2018.

Piccolroaz, S., Calamita, E., Majone, B., Gallice, A., Siviglia, A., and Toffolon, M.: Prediction of river water temperature: a comparison between a new family of hybrid models and statistical approaches, Hydrol. Process., 30, 3901–3917, https://doi.org/10.1002/hyp.10913, 2016.

Rey, D. M., Hinckley, E.-L. S., Walvoord, M. A., and Singha, K.: Integrating observations and models to determine the effect of seasonally frozen ground on hydrologic partitioning in alpine hillslopes in the Colorado Rocky Mountains, USA, Hydrol. Process., 35, e14374, https://doi.org/10.1002/hyp.14374, 2021.

Saberi, L., McLaughlin, R. T., Ng, G.-H. C., La Frenierre, J., Wickert, A. D., Baraer, M., Zhi, W., Li, L., and Mark, B. G.: Multi-scale temporal variability in meltwater contributions in a tropical glacierized watershed, Hydrol. Earth Syst. Sci., 23, 405–425, https://doi.org/10.5194/hess-23-405-2019, 2019.

Santos, A. C., Portela, M. M., Rinaldo, A., and Schaefli, B.: Analytical flow duration curves for summer streamflow in Switzerland, Hydrol. Earth Syst. Sci., 22, 2377–2389, https://doi.org/10.5194/hess-22-2377-2018, 2018.

Somers, L. D. and McKenzie, J. M.: A review of groundwater in high mountain environments, WIREs Water, 7, e1475, https://doi.org/10.1002/wat2.1475, 2020.

Somers, L. D., McKenzie, J. M., Mark, B. G., Lagos, P., Ng, G.-H. C., Wickert, A. D., Yarleque, C., Baraër, M., and Silva, Y.: Groundwater Buffers Decreasing Glacier Melt in an Andean Watershed—But Not Forever, Geophys. Res. Lett., 46, 13016–13026, https://doi.org/10.1029/2019GL084730, 2019.

Staudinger, M. and Seibert, J.: Predictability of low flow – An assessment with simulation experiments, J. Hydrol., 519, 1383–1393, https://doi.org/10.1016/j.jhydrol.2014.08.061, 2014.

Staudinger, M., Weiler, M., and Seibert, J.: Quantifying sensitivity to droughts – an experimental modeling approach, Hydrol. Earth Syst. Sci., 19, 1371–1384, https://doi.org/10.5194/hess-19-1371-2015, 2015.

https://doi.org/10.5194/egusphere-2022-921
Preprint. Discussion started: 20 September 2022

Staudinger, M., Stoelzle, M., Seeger, S., Seibert, J., Weiler, M., and Stahl, K.: Catchment water storage variation with elevation, Hydrol. Process., 31, 2000–2015, https://doi.org/10.1002/hyp.11158, 2017.

Staudinger, M., Seeger, S., Herbstritt, B., Stoelzle, M., Seibert, J., Stahl, K., and Weiler, M.: The CH-IRP data set: a decade of fortnightly data on δ^2H and δ^{18}O in streamflow and precipitation in Switzerland, Earth Syst. Sci. Data, 12, 3057–3066, https://doi.org/10.5194/essd-12-3057-2020, 2020.

Stockinger, M., Reemt Bogena, H., Lücke, A., Stumpp, C., and Vereecken, H.: Time variability and uncertainty in the fraction of young water in a small headwater catchment, Hydrol. Earth Syst. Sci., 23, 4333–4347, https://doi.org/10.5194/hess-23-4333-2019, 2019.

Tromp-van Meerveld, H. J. and McDonnell, J. J.: Threshold relations in subsurface stormflow: 1. A 147-storm analysis of the Panola hillslope, Water Resour. Res., 42, https://doi.org/10.1029/2004WR003778, 2006.

Weingartner, R. and Aschwanden, H.: Abflussregimes als Grundlage zur Abschätzung von Mittelwerten des Abflusses, Hydrol. Atlas Schweiz, Tafel 5.2, 1992.

Williams, M. W., Wilson, A., Tshering, D., Thapa, P., and Kayastha, R. B.: Using geochemical and isotopic chemistry to evaluate glacier melt contributions to the Chamkar Chhu (river), Bhutan, Ann. Glaciol., 57, 339–348, https://doi.org/10.3189/2016AoG71A068, 2016.

Wilson, A. M., Williams, M. W., Kayastha, R. B., and Racoviteanu, A.: Use of a hydrologic mixing model to examine the roles of meltwater, precipitation and groundwater in the Langtang River basin, Nepal, Ann. Glaciol., 57, 155–168, https://doi.org/10.3189/2016AoG71A067, 2016.

Zuecco, G., Penna, D., and Borga, M.: Runoff generation in mountain catchments: long-term hydrological monitoring in the Rio Vauz Catchment, Italy, Cuad. Investig. Geográfica, 44, 397–428, https://doi.org/10.18172/cig.3327, 2018.

Zuecco, G., Carturan, L., De Blasi, F., Seppi, R., Zanoner, T., Penna, D., Borga, M., Carton, A., and Dalla Fontana, G.: Understanding hydrological processes in glacierized catchments: Evidence and implications of highly variable isotopic and electrical conductivity data, Hydrol. Process., 33, 816–832, https://doi.org/10.1002/hyp.13366, 2019.